Graduate School Form
30 Updated 12/26/2015

PURDUE UNIVERSITY
GRADUATE SCHOOL
Thesis/Dissertation Acceptance

This is to certify that the thesis/dissertation prepared

By Min Wu

Entitled

STUDIES OF SULFUR-BASED CATHODE MATERIALS FOR RECHARGEABLE LITHIUM BATTERIES

For the degree of Master of Science in Mechanical Engineering

Is approved by the final examining committee:

Yongzhu Fu
Chair

Jian Xie

Likun Zhu

To the best of my knowledge and as understood by the student in the Thesis/Dissertation Agreement, Publication Delay, and Certification Disclaimer (Graduate School Form 32), this thesis/dissertation adheres to the provisions of Purdue University's "Policy of Integrity in Research" and the use of copyright material.

Approved by Major Professor(s): Yongzhu Fu

Approved by: Sohel Anwar 4/21/2016

Head of the Departmental Graduate Program Date

STUDIES OF SULFUR-BASED CATHODE MATERIALS FOR RECHARGEABLE LITHIUM BATTERIES

A Thesis

Submitted to the Faculty

of

Purdue University

by

Min Wu

In Partial Fulfillment of the

Requirements for the Degree

of

Master of Science in Mechanical Engineering

May 2016

Purdue University

Indianapolis, Indiana

Dedicated to Heping Wu, Zulian Wan, Lingling Xia, and Ling Wu, Love you forever.

ACKNOWLEDGMENTS

I would like to express my deep gratitude to my advisor, Prof. Yongzhu Fu, for his inspiring guidance and continuing support during my graduate study at Indiana University-Purdue University Indianapolis. Prof. Fu is a disciplined, thoughtful and creative researcher, who not only teaches me how to do research in the energy storage field, but also shows me the most important characters for an outstanding researcher: industrious, critical thinking and cooperation capability. Without his valuable guidance, I cannot have developed my research work successfully. I wish him every success in the future. Also, I want to express my appreciation to all my committee members, Prof. Jian Xie and Prof. Likun Zhu. They agreed to serve as my committee without any hesitation and gave me worthwhile suggestions on my thesis.

I want to thank my lab mates, Yi Cui, Amruth Bhargav, and Shravan Patil, for their kind help and inspiring discussions in my study on various aspects. I am also grateful to my collaborators, Dr. Yaroslav Losovyj, Dr. Amanda Siegel, and Dr. Jake Mosely for the technical support and assistance.

Finally, I want to express my special acknowledgement to my parents, Heping Wu and Zulian Wan, my girlfriend, Lingling Xia, and my sister, Ling Wu. Without your love and support, I cannot gain my M.S. in the United States. I love you all forever.

TABLE OF CONTENTS

Page

LIST OF FIGURES v

ABSTRACT vii

1. INTRODUCTION 1
   1.1 Li_2S Cathode 2
   1.2 Organic Cathode 4

2. LI_2S NANOCRYSTALS CONFINED IN FREE-STANDING CARBON PAPER FOR HIGH PERFORMANCE LITHIUM-SULFUR BATTERIES . 5
   2.1 Introduction 5
   2.2 Experimental Section 6
      2.2.1 Materials 6
      2.2.2 Preparation of MWCNT and CNF Paper 7
      2.2.3 Preparation of Nano-Li_2S/MWCNT and Nano-Li_2S/CNF Paper Electrodes and Cell Assembly 7
      2.2.4 Physical Characterizations 8
      2.2.5 Electrochemical Characterizations 8
   2.3 Results and Discussion 9
   2.4 Conclusions 16

3. DIMETHYL TRISULFIDE, A HIGH ENERGY DENSITY CATHODE MATERIAL FOR RECHARGEABLE LITHIUM BATTERIES 19
   3.1 Introduction 19
   3.2 Experimental Section 20
      3.2.1 Materials 20
      3.2.2 Preparation of MWCNT Paper 21
      3.2.3 Electrolyte and DMTS Catholyte Preparation 21
      3.2.4 DMTS Cell Fabrication 21
      3.2.5 Lithium Polysulfide Cell Fabrication 22
      3.2.6 Characterizations 22
   3.3 Results and Discussion 24
   3.4 Conclusions 36

4. CONCLUSIONS 38
   4.1 Li_2S Cathode 38
   4.2 Organotrisulfide Cathode 38

LIST OF REFERENCES 40

LIST OF FIGURES

Figure Page

1.1 a) Schematic of the structure of a Li_2S/Si battery and specific energy comparison of different Li-ion battery systems [5]. Copyright 2010, American Chemical Society. 3

2.1 (a) Schematic illustration of the preparation procedure of the nano-Li_2S/ MWCNT paper electrode and cell configuration; (b) XRD pattern of the blank MWCNT paper and nano-Li_2S/ MWCNT electrode; (c) curve fitting of the first peak in part b. 10

2.2 (a and b) SEM images of the pristine MWCNT paper, (c-e) SEM images of the freshly made nano-Li_2S/ MWCNT paper electrode, and EDX mapping of carbon (f) and sulfur (g) in part e. 12

2.3 (a) CV of the nano-Li_2S/MWCNT electrode cycling between 1.6 and 3.0 V at a voltage scanning rate of 0.05 mV s^{-1}; (b) voltage profile, the cell was first charged at C/20 rate and then cycled at C/10 rate; (c) Nyquist plots of a cell with a nano-Li_2S/MWCNT paper electrode after freshly made (black) and after first cycle (red); (d) cyclability and Coulombic efficiency of cells at C/5, C/2, and 1C rates; (e) rate performance; (f) typical voltage versus specific capacity profiles. All the capacity are in terms of the mass of Li_2S. 13

2.4 (a) Cyclability of the cells with different Li_2S loadings at C/10 rate; (b) Voltage versus time profile of two nano-Li_2S/MWCNT paper electrodes with different Li_2S loadings. For the Li_2S loading of 1.8 mg cm^{-2}, the cell was first charged at the C/20 rate, and then cycled between 1.8 and 3.0 V at the C/10 rate; for the Li_2S loading of 3.6 mg cm^{-2}, the cell was first charged at the C/50 rate, and then cycled between 1.65 and 3 V at the C/10 rate; (c) Voltage versus specific capacity profiles of the 5th cycles of cells with different Li_2S loadings (0.9, 1.8, and 3.6 mg cm^{-2}) at the C/10 rate. 16

2.5 (a) SEM images of the pristine CNF paper; (b and c) SEM image of the freshly made nano-Li_2S/CNF electrode; EDX mapping of carbon (d) and sulfur (e) in part c; (f) voltage profile of the nano-Li_2S/CNF electrode, the cell was first charged at C/20 rate and then cycled at C/5 rate; (g) cyclability and Coulombic efficiency of the cell at C/5 rate. The capacity values are in terms of the mass of Li_2S. 17

Figure Page

3.1 a) The possible redox reaction of DMTS; b) Schematic illustration of the cell configuration and the addition of DMTS catholyte into MWCNT paper electrode; c) The voltage-time profile of the cell with $LiNO_3$ containing ether electrolyte cycled between 1.7 - 2.7 V at C/10 rate. 25

3.2 Cyclic voltammogram of the DMTS catholyte cycling between 1.7 - 2.7 V at a voltage scanning rate of 0.02 mV s^{-1}. 26

3.3 a) XRD pattern of the discharged electrode of DMDS, the discharged and recharged electrode of DMTS; b) SEM image of the surface of the recharged electrode of DMTS after washed by DME, the inset image is the EDS analysis; c) XPS analysis of the incomplete discharged (a), and complete discharged DMTS (b), and the commercial Li_2S (c); d) GC-MS spectra of pure DMTS, the incomplete discharged electrode, and recharged electrode of DMTS. 27

3.4 Mass spectra of a) dimethyl disulfide; b) dimethyl trisulfide; c) dimethyl tetrasulfide. 29

3.5 The reaction of CH_3S radical, lithium cation, electron, and its corresponding molecular orbital. 30

3.6 a) The cycling performance and Coulombic efficiency of a cell cycled between 1.7 - 2.7 V at C/10 rate; b) The corresponding voltage-capacity profile after different cycles; c) Rate performance of a cell cycled at C/10, C/5, C/2, and 1C rates; d) The cyclability and Coulombic efficiency of a cell cycled between 1.7 - 2.7 V at C/10 rate with DMTS loading of 11.3 mg cm^{-2}. 32

3.7 Typical voltage versus specific capacity profiles of DMTS cell at different rates. 33

3.8 a) The photograph of 0.75 M Li_2S_6 solution (4.5 M sulfur) in anhydrous ethanol; b) the cycling performance and coulombic efficiency of the high loading Li-S batteries at C/10 rate. 34

3.9 SEM image of the surface morphology of a) pristine MWCNT paper; b-d) Discharged electrode of after 70 cycles; Elemental mapping of e) carbon; f) sulfur; g) overlapped carbon and sulfur. 35

3.10 a) Comparison of theoretical specific energy of some rechargeable lithium batteries ($LiCoO_2$/graphite [2], $LiFePO_4$/graphite [5], Li-I_2 [96], Li/anthraquinone [15]) with the Li/DMTS battery; b) The specific energies two cells with different electrolyte/DMTS ratios after five cycles, the specific energy density is calculated based on either the mass of lithium and DMTS or the mass of electrodes and electrolyte. 36

ABSTRACT

Wu, Min. M.S.M.E., Purdue University, May 2016. Studies of Sulfur-based Cathode Materials for Rechargeable Lithium Batteries. Major Professor: Yongzhu Fu.

Developing alternative cathodes with high capacity is critical for the next generation rechargeable batteries to meet the ever-increasing desires of global energy storage market. This thesis is focused on two sulfur-based cathode materials ranging from inorganic lithium sulfide to organotrisulfide.

For lithium sulfide cathode, we developed a nano-Li_2S/MWCNT paper electrode through solution filtration method, which involved a low temperature of 100 °C. The Li_2S nanocrystals with a size less than 10 nm were formed uniformly in the pores of carbon paper network. These electrodes show an unprecedented low overpotential (0.1 V) in the first charges, also show high discharge capacities, good rate capability, and excellent cycling performance. This superior electrochemical performance makes them promising for use with lithium metal-free anodes in rechargeable Li-S batteries for practical applications.

For organotrisulfide cathode, we use a small organotrisulfide compound, e.g. dimethyl trisulfide, to be a high capacity and high specific energy organosulfide cathode material for rechargeable lithium batteries. Based on XRD, XPS, SEM, and GC-MS analysis, we investigated the cell reaction mechanism. The redox reaction of DMTS is a $4e^-$ process and the major discharge products are $LiSCH_3$ and Li_2S. The following cell reaction becomes quite complicated, apart from the major product DMTS, the high order organic polysulfide dimethyl tetrasulfide (DMTtS) and low order organic polysulfide dimethyl disulfide (DMDS) are also formed and charged/discharged in the following cycles. With a $LiNO_3$ containing ether-based electrolyte, DMTS cell delivers an initial discharge capacity of 720 mAh g^{-1} and retains 74% of the initial

capacity over 70 cycles with high DMTS loading of 6.7 mg cm^{-2} at C/10 rate. When the DMTS loading is increased to 11.3 mg cm^{-2}, the specific energy is 1025 Wh kg^{-1} for the active materials (DMTS and lithium) and the specific energy is 229 Wh kg^{-1} for the cell including electrolyte. Adjusting on the organic group R in the organotrisulfide can achieve a group of high capacity cathode materials for rechargeable lithium batteries.

1. INTRODUCTION

The Energy storage market is increasing steadily over the last decades. As energy consumption increases, concerns about environmental pollution associated with the use of fossil fuel are becoming serious. To ease these issues, alternate energy technologies based on renewable sources like solar, wind, and electrochemical energies need to be developed and adopted [1]. Among the various energy techniques, rechargeable lithium batteries are playing an increasingly role because of their high energy density [2]. Since the introduction in 1991, lithium ion (Li-ion) batteries have become prominent in both scientific and practical fields. The conventional Li-ion batteries are based on lithium intercalation chemistry of anode and cathode materials, which limit their energy density [2,3]. A further increase in energy density requires to increase in the capacity of the anode and cathode materials or an increase in the cell operation voltage or both. However, it is unlikely to increase the cathode operating voltage beyond ∼4.3 V due to the limited electrochemical-stability window of the available liquid electrolytes [4]. Also, the capacities of the Li-insertion-oxide cathodes have reached a maximum of ∼250 mAh g^{-1}. Therefore, alternate cathode materials with higher capacity need to be developed. To overcome the charge-storage limitations of Li-insertion-oxide electrodes, materials that undergo lithium conversion reactions are becoming a promising option. In this perspective, sulfur and organic cathode materials are promising candidates for rechargeable lithium batteries [3].

Sulfur, an abundant element in earth's crust, with a high theoretical capacity of 1672 mAh g^{-1}, is considered as one of the most promising cathode materials [2]. The chemistry of a Li-S battery is fundamentally different from that of the conventional Li-ion batteries, which is based on the conversion reaction between sulfur and lithium sulfide (Li_2S) involving two electrons per sulfur atom. This different mechanism offers both significant advantages like high capacity but also generates some serious

challenges. For instance, during the lithiation step, Li-S batteries suffer from a large ($\approx$ 80%) volumetric expansion due to the conversion from sulfur (2.07 g cm^{-3}) to lithium sulfide (1.66 g cm^{-3}) [3]. Also, because of the lack of lithium in the sulfur cathode before cycling, lithium metal is usually used as the anode which has safety and cyclability issues, impeding the commercialization of Li-S batteries [5]. In this regard, lithium sulfide (Li_2S), the fully lithiated state of sulfur with a theoretical capacity of 1166 mAh g^{-1}, is a more desirable cathode material compared to sulfur as it could allow lithium-free anodes to be used, such as graphite, Si, Sn, and metal oxides [5].

1.1 Li_2S Cathode

Recently, Li_2S cathode material has attracted great interests due to its advantages of the capability of coupling with lithium-free anodes as well as the high theoretical capacity (1166 mAh g^{-1}). Yang et al. make a full cell with Li_2S cathode and silicon anode, the theoretical capacity is much higher than those of the conventional Li-ion batteries, as displayed in Figure 1.1 [5]. Although Li_2S has been generally regarded as electrochemically inactive due to its ionic and electronic insulating characteristics, significant progress has been made recently in terms of its activation and utilization. Yang et al. revealed the activation mechanism of Li_2S through thermodynamic and electrochemical analysis [5]. They found the activation is largely related to charge transfer kinetics and can be overcame by utilizing higher operation voltage. In the following cycles, the cell voltage becomes the normal operation voltage of Li-S batteries.

Nevertheless, the large overpotential ($\sim$1 V) still causes some drawbacks to use Li_2S cathode material [6]. First, the activation is very difficult to be entirely achieved, which limits the cell capacity. Also, it always requires a high cutoff voltage of $\sim$4.0 V in the first charge to activate the micro-sized Li_2S particles. At this high potential,

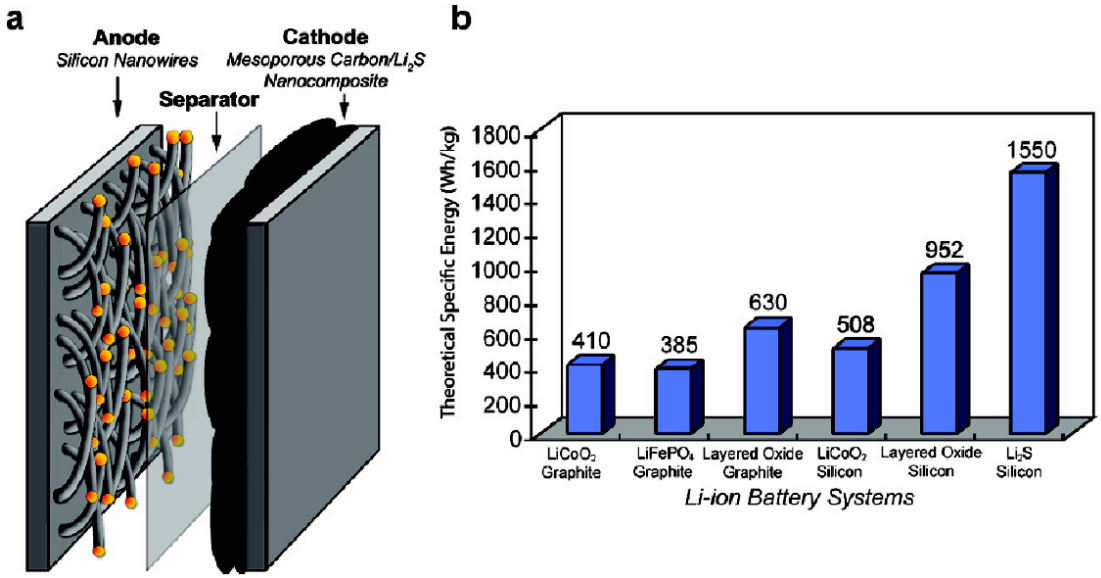

Figure 1.1. a) Schematic of the structure of a Li_2S/Si battery and specific energy comparison of different Li-ion battery systems [5]. Copyright 2010, American Chemical Society.

the commonly used ether-based electrolytes in Li-S batteries become unstable which depreciates their electrochemical performance [7].

More recently, several researches focused on decreasing the activation barrier of Li_2S and improving its discharge capacity. Aurbach et.al first introduced some redox mediators, including lithium iodine, ferrocene, and decamethylferrocene [6]. With the assistance of redox mediators, the Li_2S cathode could be activated most its charge capacity at around 3 V for microsized Li_2S particles. Later, Zu et al. developed a P_2S_5 electrolyte additive to activate the micro-sized Li_2S cathode [8]. With the use of P_2S_5 containing electrolyte, the over-potential decreased to 0.3 V. The initial discharge capacity is up to 800 mAh g^{-1}. Besides, in-situ synthesized Li_2S cathode developed by Fu et al. also shows a negligible overpotential perhaps due to the amorphous Li_2S [9]. Although great progresses have been made on Li_2S cathode, it still faces a lot of challenges including the relative low utilization and rapid capacity fading, so more researches are needed to address these challenges.

1.2 Organic Cathode

Organic electrode materials are considered as promising alternative electrode materials for rechargeable batteries because of the high theoretical capacity, safety, sustainability, environmental benignity, and low cost [10, 11]. In addition, the unique characteristics of organic compounds, like structural diversity and flexibility, make them promising candidates for electrodes of rechargeable Li batteries [12–16], supercapacitors [17], and redox flow batteries [18].

Among all the organic electrode materials, three types including free radical compounds, carbonyl compounds, and organosulfur compounds are investigated the most [10,11]. For quinone electrode materials, normally both the charge and discharge products could dissolve in electrolyte, leading to a fast capacity fading [15, 16, 19]. In 1988, Visco et al. first studied the tetraethylthiuram disulfide as cathode materials for high temperature sodium battery [20]. They found that the S-S bond can be reversibly broken and rebuilt, and a two-electron redox reaction were involved. Later, they proposed the disulfide/thiolate mechanism for the organodisulfide cathode. Whereafter, a lot of studies on organodisulfide cathode materials were published, including the dimeric organodisulfides and polymeric organodisulfides. Although huge efforts were made in optimizing the polymer structure and introducing electrocatalytic additives, the intrinsic drawbacks like dissolution and slow kinetics seemed unlikely to be overcome completely. Also, the electrochemical performance was difficult to achieve a satisfactory level for practical use.

2. LI_2S NANOCRYSTALS CONFINED IN FREE-STANDING CARBON PAPER FOR HIGH PERFORMANCE LITHIUM-SULFUR BATTERIES

2.1 Introduction

High energy rechargeable batteries are in increasingly high demand owing to the increasing use of electric vehicles and portable electronics. Lithium-sulfur (Li-S) batteries, with a high theoretical specific capacity of sulfur (i.e., $\sim$1672 mAh g^{-1}), are considered as a promising high energy density substitute of traditional lithium-ion batteries [2, 21–23]. Sulfur as a cathode material has many benefits, such as abundance, low cost, high energy, and environmental benignity. Because of the lack of lithium in the sulfur cathode before cycling, lithium metal is usually used as the anode which has safety and cyclability issues [24–27], impeding the commercialization of Li-S batteries. In this regard, lithium sulfide (Li_2S), the fully lithiated state of sulfur with a theoretical capacity of 1166 mAh g^{-1}, is a more desirable cathode material compared to sulfur as it could allow lithium-free anodes to be used, such as graphite, Si, Sn, and metal oxides [5, 9, 28–36]. Due to the low electronic conductivity, low lithium-ion diffusivity, and high charge transfer resistance of lithium sulfide, a large overpotential ($\sim$1 V) was usually observed in the initial activation of micrometer-sized Li_2S particles, which requires a high cutoff voltage of $\sim$4.0 V in the first charge [37,38]. At this high potential, the commonly used ether-based electrolytes in Li-S batteries could be unstable and deteriorate their electrochemical performance [7].

Recently, several Li_2S cathodes with low initial overpotential have been developed. To decrease the activation barrier of Li_2S, there are two main strategies. One is to use electrolyte additives [6, 8, 37, 39, 40], e.g., lithium polysulfide [37, 39], redox mediators [6], LiI [6, 40], and P_2S_5 [8]; however, the effect of decreasing overpotential is not very satisfactory. The other one is to reduce Li_2S particle size to the

nanoscale [31, 34, 35, 41–45]. Unfortunately, Li_2S is highly sensitive to moisture and has a high melting point of 938 °C [46, 47], which makes it difficult to synthesize Li_2S nanoparticles. In addition, like sulfur, Li_2S also has the issue of polysulfide shuttle in Li-S cells. To fulfill the high capacity of Li_2S, a good current collector (e.g., carbon) with a favorable nanostructure which can hold polysulfides is needed in the Li_2S cathode. Currently, chemical synthesis of Li_2S-carbon nanocomposites requires multistep sophisticated processes [31, 40, 42–44], including high temperature carbonization in an inert atmosphere to protect Li_2S from moisture, which are not scalable. To enable Li_2S cathodes for practical applications, a simple and scalable method is needed.

Herein, we present a facile method to uniformly distribute Li_2S nanoparticles into binder-free, free-standing multiwalled carbon nanotube (MWCNT) and carbon nanofiber (CNF) paper current collectors by a Li_2S solution filtration method. The prepared electrodes are designated as nano-Li_2S/MWCNT and nano-Li_2S/CNF, respectively. This approach is inspired from our previous work on the highly reversible Li/dissolved polysulfide cell using a MWCNT paper current collector [48]. The Li_2S nanoparticles with a size of less than 10 nm are formed in the pores of carbon paper, regardless of the pore size in the carbon network. These electrodes show an unprecedented low overpotential in the first charge, high discharge capacities, good rate capability, and excellent cycling performance. This process is under low temperature, and high Li_2S loading can be achieved, making it a low cost, scalable approach.

2.2 Experimental Section

2.2.1 Materials

Lithium trifluoromethanesulfonate ($LiCF_3SO_3$, 98%, Acros Organics), lithium nitrate ($LiNO_3$, 99+%, Acros Organics), dimethoxy ethane (DME, 99+%, Acros Organics), 1,3-dioxolane (DOL, 99.5%, Acros Organics), lithium sulfide (Li_2S, 99.98%, Sigma-Aldrich), and anhydrous ethanol (99.5%, Sigma-Aldrich) were purchased and used as received.

2.2.2 Preparation of MWCNT and CNF Paper

An 80 mg portion of MWCNTs (Nanostructure and Amorphous Materials, Inc.) was dispersed in a miscible solution of deionized water (700 mL) and isopropyl alcohol (20 mL) by ultrasonication for 10 min, followed by vacuum filtration to render a free-standing MWCNT paper. The MWCNT paper was dried in an air-oven for 24 h at 100 °C before being peeled off and punched out into circular disks with 1.2 cm diameter (1.13 cm^2 in area, 2.2-2.4 mg in mass) for use as the current collector. The preparation of CNF (Sigma-Aldrich) paper is similar to that of the MWCNT paper.

2.2.3 Preparation of Nano-Li_2S/MWCNT and Nano-Li_2S/CNF Paper Electrodes and Cell Assembly

An appropriate amount of commercial lithium sulfide powder was dissolved in anhydrous ethanol in an argon-filled gloved box to form a 0.5 M Li_2S solution. The MWCNT paper was further dried at 100 °C under vacuum for 10 h to remove moisture before the preparation of nano-Li_2S/MWCNT paper electrode. First, 15 μL of Li_2S solution was added into the MWCNT paper, and then the nano-Li_2S/MWCNT electrode was dried at 40 °C inside the glovebox. The nano-Li_2S/MWCNT electrode was flipped, and additional Li_2S solution was added, and then the electrode was dried again. This procedure was repeated three times until the mass of Li_2S in the electrode was calculated to be 1 mg, corresponding to 0.9 mg cm^{-2} in the electrode. Finally, the nano-Li_2S/MWCNT electrode was dried at 100 °C in the gloved box for another 5 h to completely remove ethanol. For the cell assembly, 20 μL of electrolyte (1.0 M $LiCF_3SO_3$/0.1 M $LiNO_3$ in DME/DOL (1:1 v/v)) was added into the nano-Li_2S/MWCNT electrode, and then a Celgard 2400 separator was placed on top of the electrode, followed by additional electrolyte and lithium metal anode. Finally the cell was crimped for electrochemical evaluation on an Arbin battery cycler. For the preparation of electrodes with a Li_2S loading of 1.8 mg cm^{-2}, the Li_2S solution filtration and drying process was repeated six times, and then the Li_2S mass was

accumulated to be 2 mg, corresponding to 1.8 mg cm^{-2} in the electrode. For the high Li_2S loading of 3.6 mg cm^{-2}, two layers of nano-Li_2S/MWCNT electrodes were stacked, and each has a Li_2S loading of 1.8 mg cm^{-2}. For the preparation of nano-Li_2S/CNF electrodes, a similar Li_2S solution filtration method was used, and the Li_2S loading is 0.9 mg cm^{-2}.

2.2.4 Physical Characterizations

The X-ray diffraction (XRD) data of the nano-Li_2S/MWCNT electrode and pristine MWCNT paper were collected on a PANalytical Empyrean X-ray diffractometer equipped with Cu Kα radiation. The samples were protected in the sample holder by Kapton tape. The scanning rate was 1° min^{-1}, and 2θ was between 20° and 80°. The XRD pattern of commercial Li_2S powder was also collected for comparison. The morphological characterizations were conducted with a JEOL JSM-7800F field emission scanning electron microscopy (SEM). The elemental mapping was performed with energy-dispersive X-ray spectroscopy (EDX) attached to the SEM.

2.2.5 Electrochemical Characterizations

In the cycling measurements, the cells with a Li_2S loading of 0.9 mg cm^{-2} were galvanostatically charged to 2.8 V at C/20 rate in the first charge with an Arbin battery cycler, then cycled between 1.8 and 2.8 V at C/10 and C/5 rates, 1.75-2.8 V at C/2 rate, 1.65-2.8 V at 1C rate, and 1.6-2.8 V at 2C rate. The dropping cutoff voltage with increasing rate is to guarantee full discharge voltage profiles due to the larger overpotential at higher rates. The cells with a Li_2S loading of 1.8 mg cm^{-2} were galvanostatically charged to 3 V at C/20 rate, and then cycled between 1.8 and 3 V at C/10. The cells with a Li_2S loading of 3.6 mg cm^{-2} were galvanostatically charged to 3 V at C/50, and then cycled between 1.65 and 3 V at C/10. The current rates and specific capacities were based on the mass of Li_2S present in the cathode (1C = 1166 mA g^{-1}). Cyclic voltammetry (CV) was performed on a Bio-Logic VSP potentiostat

from open circuit voltage to 3.0 V, and then cycled between 3 and 1.6 V versus Li^+/Li at a scanning rate of 0.05 mV s^{-1}. Electrochemical impedance spectroscopy (EIS) data were collected with a Bio-Logic VSP impedance analyzer in the frequency range of 100 kHz-0.1 Hz with an applied voltage of 5 mV and Li foil as the counter and reference electrode.

2.3 Results and Discussion

The preparation procedure of the electrode is illustrated in Figure 2.1a. First, commercial Li_2S powder was dissolved in anhydrous ethanol to form a homogeneous solution with a concentration of 0.5 M Li_2S, as reported by Wu et al [49]. Subsequently, a specific amount of the Li_2S solution was added into a disc of MWCNT paper, followed by drying in an argon-filled glovebox ($<$ 1 ppm of H_2O). Since the MWCNT paper has a strong absorbency to ethanol, the Li_2S solution could infiltrate throughout the MWCNT paper. Upon the evaporation of ethanol solvent, Li_2S started to nucleate. The one-dimensional (1D) structure of MWCNTs could provide nucleation sites for the formation of Li_2S particles, and the 3D porous structure of the MWCNT paper impedes Li_2S particles from agglomeration into microsized particles; therefore, the formed Li_2S particles can be in nanoscale and be uniformly dispersed in the network of the MWCNT paper.

X-ray diffraction (XRD) was performed to confirm the crystal structure of the nano-Li_2S/MWCNT electrode, and the XRD pattern is shown in Figure 2.1b. The XRD diffractions of Li_2S (JCPSD 65-2981) and the pristine MWCNT paper are also presented for comparison. The main peak of MWCNT is centered at around $2\theta = 26.0°$, which is known as the (002) crystal plane of carbon nanotubes [1]. The highest peak of Li_2S is at $2\theta = 27.4°$, which overlaps with the (002) plane peak of MWCNT. Figure 2.1c shows the curve fitting of the first peak in Figure 2.1b. The two deconvoluted peaks can be assigned to the (002) plane peak of MWCNT at 26.0° and the (111) plane peak of Li_2S at 27.4°, respectively. The other three major

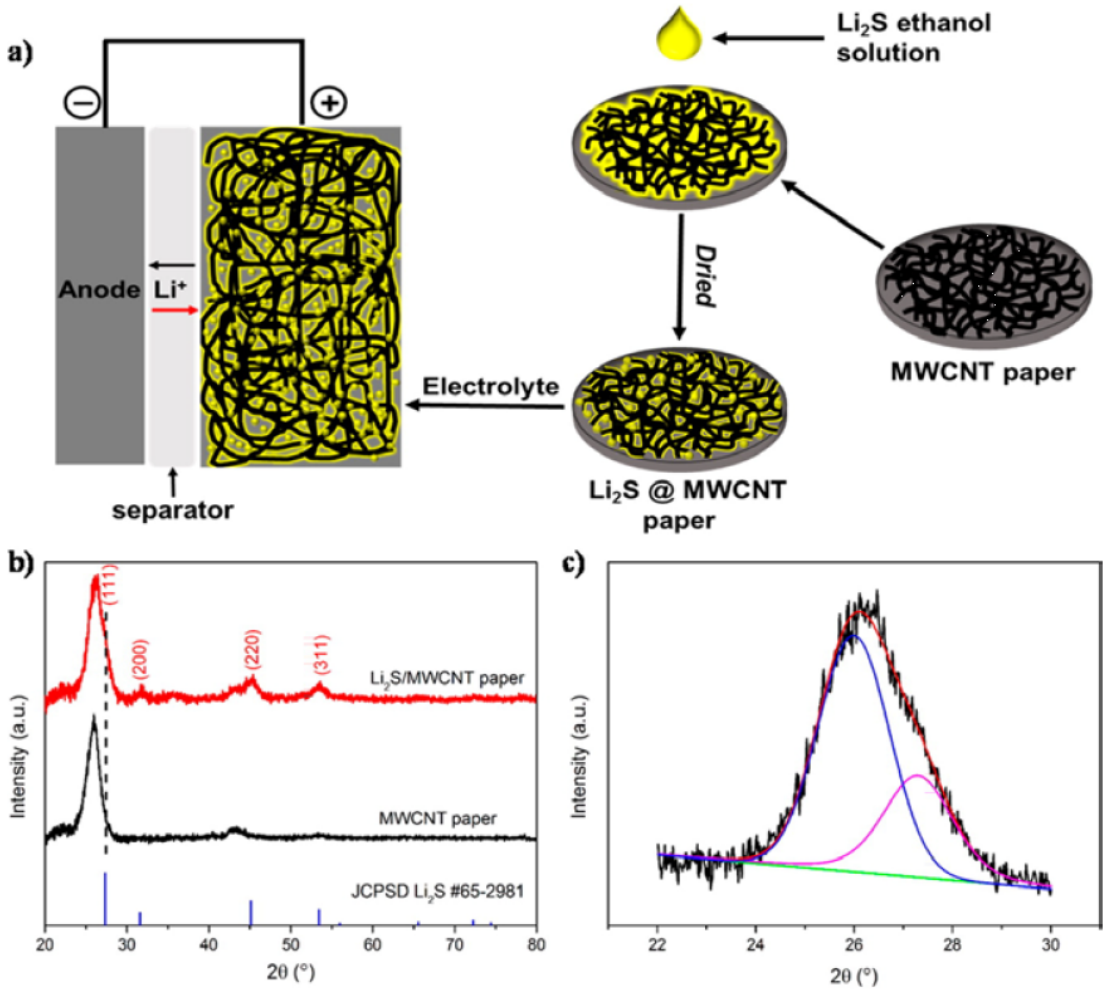

Figure 2.1. (a) Schematic illustration of the preparation procedure of the nano-Li_2S/ MWCNT paper electrode and cell configuration; (b) XRD pattern of the blank MWCNT paper and nano-Li_2S/ MWCNT electrode; (c) curve fitting of the first peak in part b.

peaks of Li_2S in Figure 2.1b match well with the PDF data. These peaks are broad, indicating the nucleated Li_2S crystals are fairly small. According to the Scherrer equation [50, 51], the calculated size of Li_2S nanocrystals is about 7.8 nm.

Scanning electron microscopy (SEM) characterization was conducted to investigate the morphology variation between the pristine MWCNT paper and the freshly made nano-Li_2S/MWCNT electrode, as shown in Figure 2.2. The top view of the pristine MWCNT paper at low magnification displays the self-weaving behavior of

MWCNTs and the nanoporous network of the MWCNT paper in Figure 2.2a. From the high magnification SEM image in Figure 2.2b, it can be seen that the diameter of MWCNTs is about 10-25 nm, and the size of pores is around 100-300 nm. Figure 2.2 (c-e) presents the SEM images of the nano-Li_2S/MWCNT electrode; the pores of the MWCNT paper were mostly filled with Li_2S nanocrystals. The whole structure of the nano-Li_2S/MWCNT electrode is still porous, which allows efficient electrolyte penetration. The MWCNTs offer nucleation and anchoring sites for the Li_2S nanocrystals, as shown by the red parallel lines in Figure 2.2d. All MWCNTs are coated with Li_2S nanocrystals, forming a core-sheath structure. Obviously, the Li_2S-coated MWCNTs in Figure 2.2d are much thicker than the pristine MWCNTs shown in Figure 2.2b. To our surprise, the Li_2S particles in the pores of the MWCNT network are actually very small, most of which are less than 10 nm, as indicated by the green arrows in Figure 2.2d. The orange circles indicate that the nanopores still exist in the electrode, which are desirable for lithium-ion transport consequently improving the electrode kinetics. The elemental mapping of carbon (Figure 2.2f) and sulfur (Figure 2.2g) evidently validate that they are homogeneously distributed in the nano-Li_2S/MWCNT electrode. Furthermore, Figure 2.2g does not show agglomerated sulfur clusters, indicating that the Li_2S particles are mostly in nanoscale.

Figure 2.3a shows the cyclic voltammogram (CV) of a half cell with the nano-Li_2S/ MWCNT electrode. The voltage was first swept from the open circuit voltage ($\sim$2.09 V) to 3 V followed by cycling between 3 and 1.6 V at a rate of 0.05 mV s^{-1}. In the first cycle, the wide anodic peak is centered at 2.48 V corresponding to the oxidation of Li_2S to polysulfides or sulfur [47]. The anodic peaks in the following cycles have shifted slightly to a lower voltage at around 2.4 V. The small potential difference (0.1 V) between the first and following cycles in CV indicates a negligible overpotential of the nano-Li_2S/ MWCNT electrode, which is significantly smaller than those of microsized Li_2S crystals reported [37, 38]. The anodic peak begins splitting into double peaks at $\sim$2.38 and $\sim$2.43 V in the third cycle, which correspond, respectively, to the transitions of Li_2S to low order polysulfides and then to high order

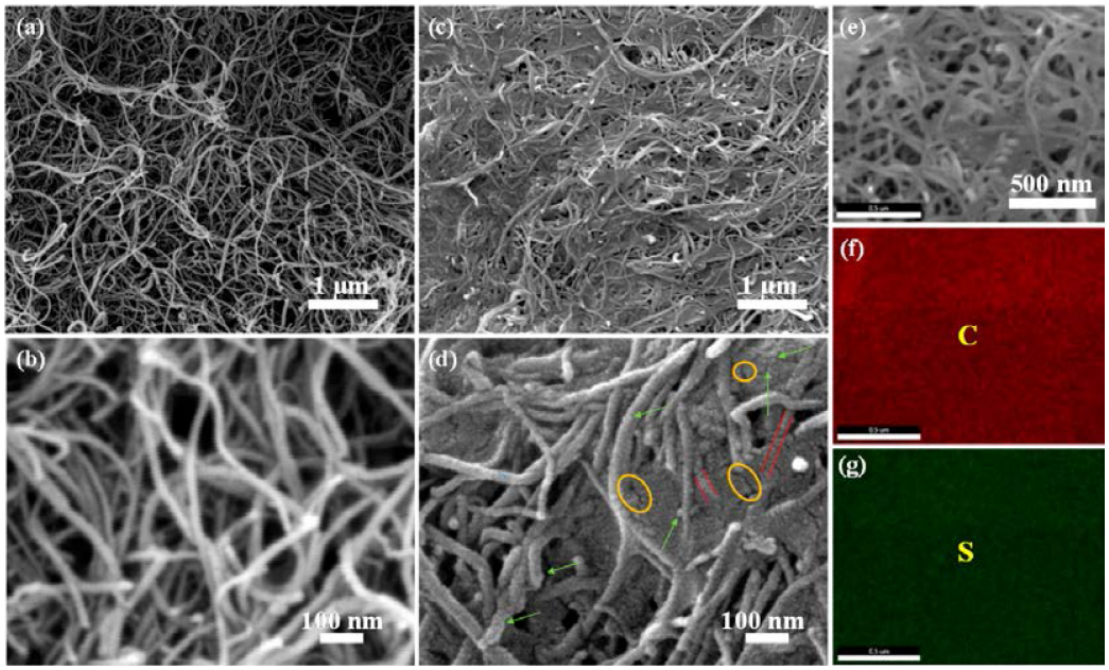

Figure 2.2. (a and b) SEM images of the pristine MWCNT paper, (c-e) SEM images of the freshly made nano-Li_2S/ MWCNT paper electrode, and EDX mapping of carbon (f) and sulfur (g) in part e.

polysulfides/sulfur [52]. In the cathodic sweep, the two peaks stay almost the same from the 2nd to the 10th cycle, revealing an excellent electrochemical stability of the nano-Li_2S/MWCNT electrode.

Figure 2.3b shows the voltage profile of the first three cycles of the nano-Li_2S/ MWCNT electrode in a half cell. The cell was first charged to 2.8 V at C/20, and then cycled between 1.8 and 2.8 V at C/10. During the first charge, the initial charge voltage is between 2.2 and 2.45 V, which is significantly lower than those with microsized Li_2S particles under similar charge conditions [25, 26, 37, 38, 43, 53–55], indicating a negligible overpotential in the nano-Li_2S/MWCNT electrode. This result is consistent with the CV shown in Figure 2.3a. The following discharge exhibits two voltage plateaus which resemble the voltage profile of conventional sulfur electrodes. To understand the impedance in the nano-Li_2S/MWCNT electrode, electrochemical impedance spectroscopy (EIS) analysis was conducted on the cell. As shown in Figure

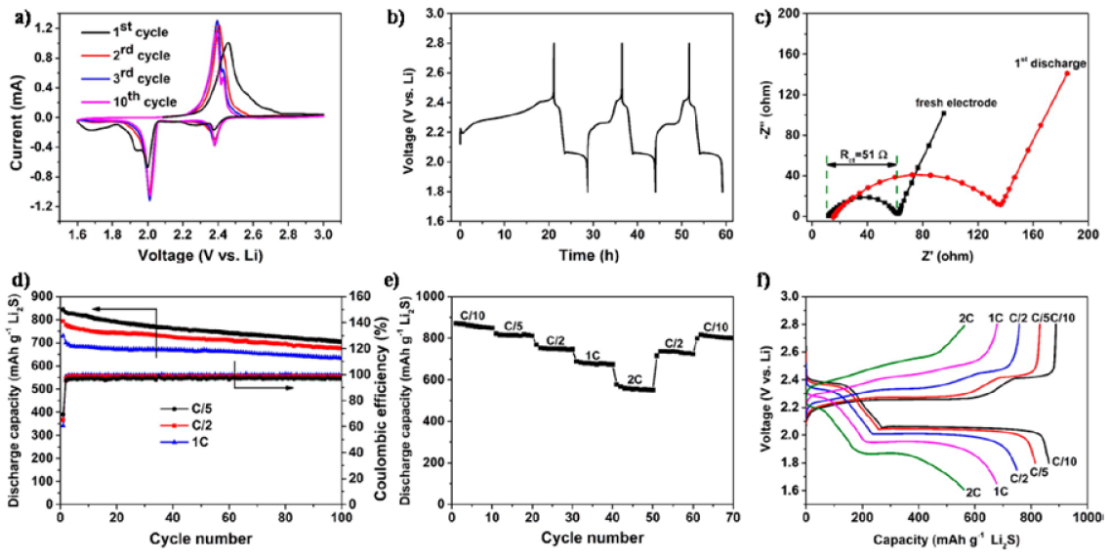

Figure 2.3. (a) CV of the nano-Li_2S/MWCNT electrode cycling between 1.6 and 3.0 V at a voltage scanning rate of 0.05 mV s^{-1}; (b) voltage profile, the cell was first charged at C/20 rate and then cycled at C/10 rate; (c) Nyquist plots of a cell with a nano-Li_2S/MWCNT paper electrode after freshly made (black) and after first cycle (red); (d) cyclability and Coulombic efficiency of cells at C/5, C/2, and 1C rates; (e) rate performance; (f) typical voltage versus specific capacity profiles. All the capacity are in terms of the mass of Li_2S.

2.3c, the charge transfer resistance (Rct) reflected by the semicircle in the high-medium frequency region in the freshly made nano-Li_2S/MWCNT electrode is only 51 Ω. In contrast, the Rct significantly increases to about 121 Ω after the first cycle (discharge). The low initial Rct indicates good contact between Li_2S nanocrystals and MWCNTs in the nano-Li_2S/MWCNT electrode, which consequently results in the low overpotenial in the first charge.

The cycling performance of the nano-Li_2S/MWCNT electrode with a Li_2S loading of 0.9 mg cm^{-2} at different C rates is shown in Figure 2.3d. The initial discharge capacities at C/5 and C/2 are 843 and 794 mAh g^{-1}, respectively. After 100 cycles, the remaining capacities are as high as 705 and 676 mAh g^{-1}, corresponding to capacity retentions of 83.6% and 85.1%, respectively. As the current density increases to 1C rate, the cycling stability improves. After the first three cycles, the discharge capacity stays as high as 92.4% from the 4th cycle to the 100th cycle, which corresponds to a

low capacity fading rate of 0.078% per cycle. Moreover, starting the second cycle, the average Coulombic efficiency is around 97-99.5% over 100 cycles. The high efficiency could be ascribed to the addition of $LiNO_3$ in the electrolyte and the good reservation of polysulfides in the MWCNT paper [48,56]. The low efficiency in the first cycle could be due to side reactions and the formation of solid electrolyte interphase (SEI) on the surface of lithium metal anode. As the rate increases from C/5 to 1C, the efficiency slightly increases; this is because high rates weaken the shuttle effect of dissolved polysulfides by reducing the retention time of polysulfides within the electrolyte per cycle [57].

Figure 2.3e presents the rate capability of the nano-Li_2S/MWCNT electrode. The cell shows high discharge capacities of 860, 814, 749, and 678 mAh g^{-1} at C/10, C/5, C/2, and 1C, respectively. Even at a high rate of 2C, the discharge capacity still can be 555 mAh g^{-1}. When the rate regained to C/10, the discharge capacity recovered to 810 mAh g^{-1} which is only marginally lower than that of the initial 10 cycles at C/10 rate, implying high reversibility of the nano-Li_2S/MWCNT electrode. Representative voltage profiles at different C-rates are shown in Figure 2.3f. It can be seen that the cell polarization (voltage difference between the first charge voltage plateau and the second discharge voltage plateau) slightly increases from 0.19 to 0.47 V as the rate increases from C/10 to 1C. At 2C rate, the second discharge voltage plateau is still at 1.87 V, which is higher than the values reported in the literature [38, 44]. The high rate capability can be attributed to the good electrode kinetics resulting from the porous nanostructure of the Li_2S/MWCNT electrode as shown in Figure 2.2.

The nano-Li_2S/MWCNT electrodes with different mass loadings of Li_2S have also been evaluated. Figure 2.4a shows the cycle life of three cells at C/10 rate with Li_2S loadings of 0.9, 1.8, and 3.6 mg cm^{-2}, which correspond to the mass proportions of Li_2S of 30, 47, and 47 wt %, respectively, in the electrodes. For the Li_2S loading of 3.6 mg cm^{-2}, the cathode consists of two layers of nano-Li_2S/MWCNT electrodes with a Li_2S loading of 1.8 mg cm^{-2} each. Figure 2.4b shows the voltage versus time profile of the first cycles of the two cells with the Li_2S loadings of 1.8 and 3.6 mg

cm^{-2}. Consistently, these two cells exhibit very low charge voltages (overpotential) in their first charge, which are lower than 2.4 V. As can be seen in Figure 2.4a, the specific capacity of Li_2S decreases as the Li_2S loading increases. For the Li_2S loading of 1.8 and 3.6 mg cm^{-2}, the initial capacities are 764 and 590 mAh g^{-1} at C/10 rate, respectively. After 50 cycles, the discharge capacities are still maintained at 705 and 576 mAh g^{-1}. A representative voltage versus capacity profile of these three cells is displayed in Figure 2.4c for comparison. For the high Li_2S loading of 3.6 mg cm^{-2}, the initial capacity is lower than those in the following cycles; this could be because inactive Li_2S particles within the high loading electrode could be utilized during the later cycling. High Li_2S loadings are essential for practical use, and the Li_2S loading of 3.6 mg cm^{-2} is one of the highest Li_2S loadings ever reported.

To demonstrate the versatility of this method for other self-weaving fibrous carbon current collectors, we also prepared and evaluated nano-Li_2S/CNF electrodes. CNFs are much thicker than MWCNTs, and they also form larger pores. Figure 2.5a shows SEM images of the pristine CNF paper. The pristine CNF paper has large pores the size of a few microns in the CNF network. After the electrode was prepared, almost all pores were filled with Li_2S crystals as shown in Figure 2.5 (b, c). Although the pores are very large, the Li_2S particles are still nanosized and agglomerate in the pores forming a nanoporous structure as shown in Figure 2.5c. The EDX spectrum in Figure 2.5e clearly shows that lithium sulfide is homogeneously distributed in the CNF network. This result demonstrates that only Li_2S nanoparticles instead of large Li_2S crystals can be formed by this solution filtration method, regardless of the pore size in the carbon network. The voltage profile of the nano-Li_2S/CNF electrode shown in Figure 2.5f is quite similar to that of the nano-Li_2S/MWCNT electrode shown in Figure 2.4b, presenting very low charge overpotential. The main charge voltage is below 2.4 V in the first cycle. With a Li_2S loading of 0.9 mg cm^{-2}, the nano-Li_2S/CNF paper electrode can deliver a high initial capacity of 827 mAh g^{-1} at C/5 rate and maintain a capacity retention of 86% over 80 cycles, as presented in

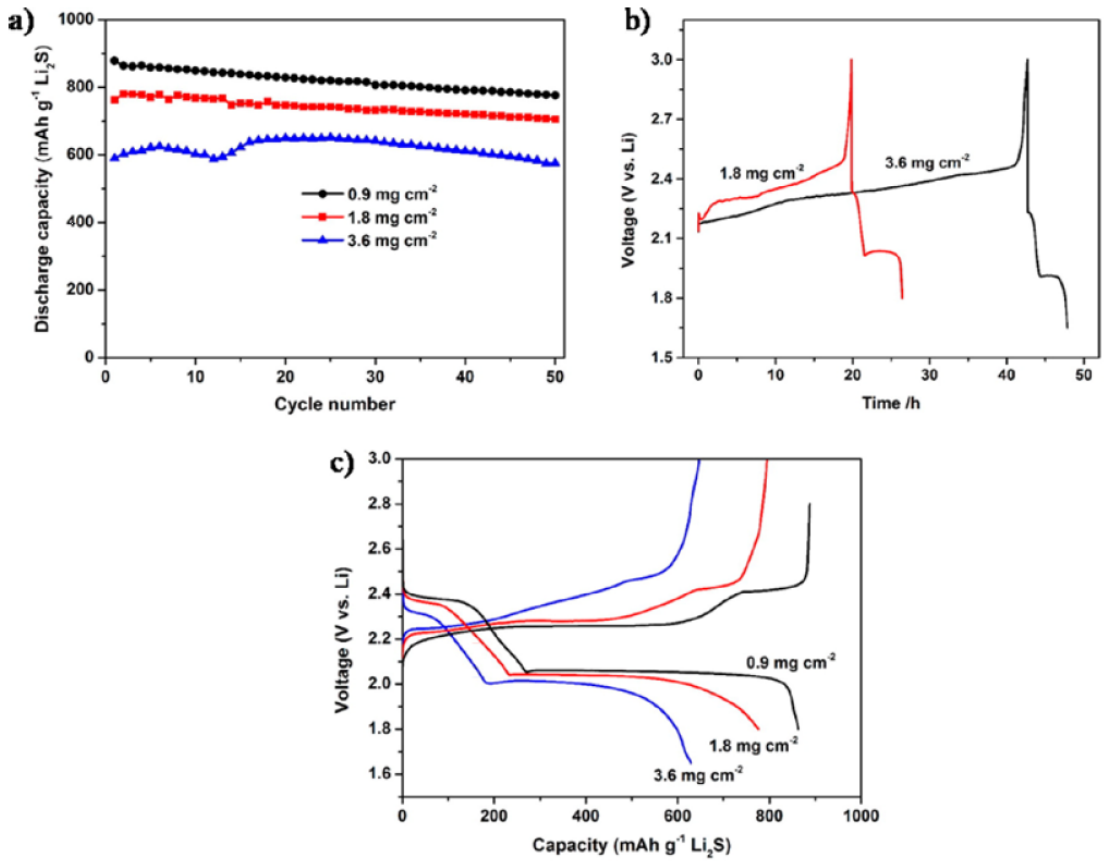

Figure 2.4. (a) Cyclability of the cells with different Li_2S loadings at C/10 rate; (b) Voltage versus time profile of two nano-Li_2S/MWCNT paper electrodes with different Li_2S loadings. For the Li_2S loading of 1.8 mg cm^{-2}, the cell was first charged at the C/20 rate, and then cycled between 1.8 and 3.0 V at the C/10 rate; for the Li_2S loading of 3.6 mg cm^{-2}, the cell was first charged at the C/50 rate, and then cycled between 1.65 and 3 V at the C/10 rate; (c) Voltage versus specific capacity profiles of the 5th cycles of cells with different Li_2S loadings (0.9, 1.8, and 3.6 mg cm^{-2}) at the C/10 rate.

Figure 2.5g. Obviously, the nano-Li_2S/CNF electrode shows comparable outstanding performance with the nano-Li_2S/MWCNT electrode.

2.4 Conclusions

In summary, we have successfully developed a binder-free, freestanding nano-Li_2S/carbon paper electrode via a simple Li_2S solution filtration method, of which the

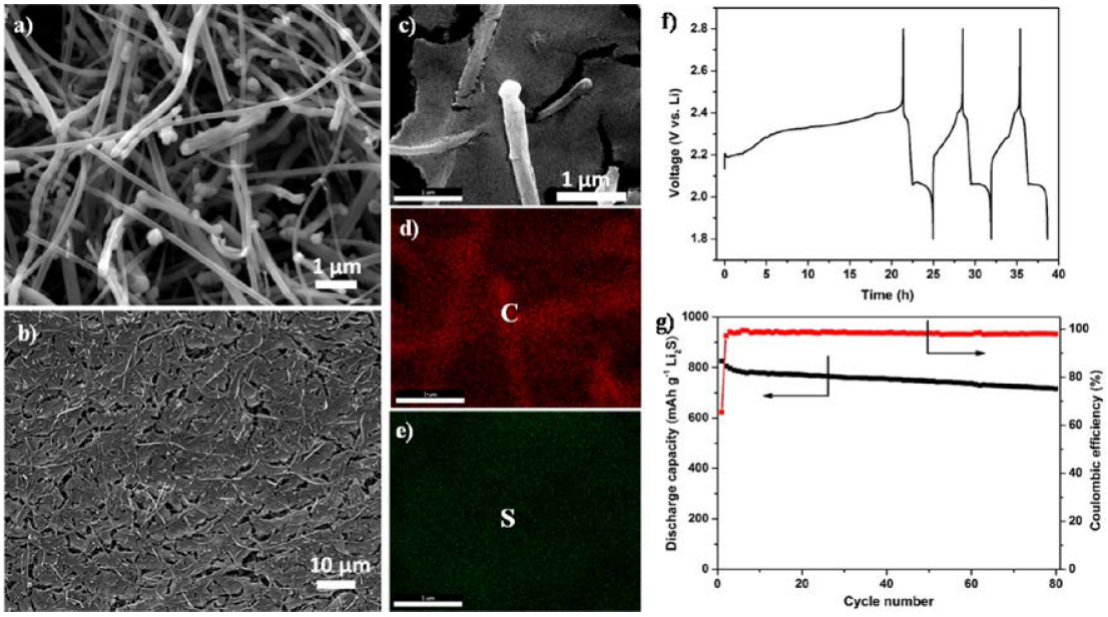

Figure 2.5. (a) SEM images of the pristine CNF paper; (b and c) SEM image of the freshly made nano-Li_2S/CNF electrode; EDX mapping of carbon (d) and sulfur (e) in part c; (f) voltage profile of the nano-Li_2S/CNF electrode, the cell was first charged at C/20 rate and then cycled at C/5 rate; (g) cyclability and Coulombic efficiency of the cell at C/5 rate. The capacity values are in terms of the mass of Li_2S.

carbon can be MWCNT or CNF. Li_2S nanocrystals are formed as small as 10 nm and are uniformly distributed in the nanoporous carbon paper framework. The nanosized Li_2S particles together with the high conductivity of the carbon paper lead to low impedance and high performance nano-Li_2S/carbon paper electrodes with negligible overpotentials in the first charge in Li-S batteries. Both electrodes demonstrate high initial capacities and excellent cycling stability. For example, the nano-Li_2S/MWCNT electrode retained a reversible capacity of 705 mAh g^{-1} with a capacity retention of 83.6% at C/5 rate over 100 cycles. With a high Li_2S loading of 3.6 mg cm^{-2}, the electrode still exhibits a reversible capacity of 576 mAh g^{-1} at C/10 rate over 50 cycles. The nano-Li_2S/CNF electrode shows comparable performance as the nano-Li_2S/MWCNT electrode with an initial discharge capacity of 827 mAh g^{-1} at C/5 rate and a capacity retention of 86% over 80 cycles. These results demonstrate a facile and scalable electrode fabrication process for making high performance nano-Li_2S/carbon

paper electrodes for high energy Li-S batteries. The superior cell performance makes them promising to be used with metal-free anodes in rechargeable Li-S batteries for practical applications.

3. DIMETHYL TRISULFIDE, A HIGH ENERGY DENSITY CATHODE MATERIAL FOR RECHARGEABLE LITHIUM BATTERIES

3.1 Introduction

Electrochemical energy storage devices are in high demand owing to the increasing use of portable electronics and electric vehicles. Rechargeable lithium batteries have attracted tremendous interest owing to their high energy density [58, 59]. Conventional rechargeable lithium batteries, also known as lithium-ion (Li-ion) batteries, are based on the lithium intercalation chemistry of anode and cathode materials [3]. However, issues like high cost, thermal instability, and in particular, insufficient energy density need to be further addressed to meet the demand of key application markets [4, 60]. To increase energy density of lithium batteries, high capacity electrodes need to be developed. In this perspective, elemental sulfur and oxygen are promising cathode materials due to their capacities of 1672 and 3350 mAh g^{-1}, respectively, which are an order of magnitude higher than those of cathodes used in Li-ion batteries. Yet, both of them have several intrinsic difficulties that should be addressed before they could be used in practical application [10]. As attractive are organic electrode materials featuring high theoretical capacity, safety, sustainability, environmental benignity, and low cost [10,11,16]. Additionally, the unique traits of organic compounds, like structure diversity, solubility and flexibility, make them promising candidates for anodes or cathodes of rechargeable Li/Na batteries [16, 61–67], supercapacitors [17], thin-film batteries [68], and redox flow batteries [18].

Among organic electrode materials, three types including free radical compounds, carbonyl compounds, and organosulfur compounds are investigated the most [10, 11]. Most organic electrode materials like quinone-based materials could dissolve in liquid electrolyte including their discharged products, resulting in fast capacity fading [14–

16, 19]. In 1988, Visco et al. first investigated organosulfide, i.e., tetraethylthiuram disulfide, as a cathode material for high temperature sodium battery [69]. They found that the S-S bond can be reversibly broken and formed upon cycling, and a $2e^-$ redox reaction occurs. Whereafter, a lot of studies on organodisulfide cathode materials were carried out, including dimeric organodisulfides [70,71], and polymeric organodisulfides [12, 13, 72–81]. Although huge efforts have been made in optimizing the polymer structure and introducing electrocatalytic additives, the intrinsic drawbacks like slow kinetics and low capacity seem unlikely to be overcome [11].

In order to develop cathodes with high capacity, high energy density, and better cycling stability, we are exploring organotrisulfide (R-S-S-S-R, R is an alkyl group) rather than organodisulfide (R-S-S-R) as a cathode material for rechargeable lithium batteries. Apart from the same advantages like solubility, feasibility, and structural diversity in organodisulfide, organotrisulfide have higher theoretical capacity and faster kinetics than organodisulfide. The extra middle sulfur atom in organotrisulfide can increase specific capacity due to two more electrons that can be stored to form lithium sulfide (Li_2S) as well as lower the dissociation energy of the S-S bond. For example, the dissociation energy of the S-S bond in dimethyl disulfide (DMDS, CH_3SSCH_3) is known to be about 70 kcal $mole^{-1}$ [82], whereas that of the S-S bond in dimethyl trisulfide (DMTS, CH_3SSCH_3) decreases to about 45 kcal $mole^{-1}$ [83]. The low dissociation energy supports fast electrode kinetics.

Herein, we use a small organotrisulfide molecule, i.e., DMTS, to demonstrate the proof-of-concept.

3.2 Experimental Section

3.2.1 Materials

Lithium bis(trifluoromethanesulfonimide) (LiTFSI, $LiN(CF_3SO_2)_2$, 99%, Acros Organics), lithium nitrate ($LiNO_3$, 99.999%, Acros Organics), 1,2-Dimethoxyethane (DME, 99.5%, Sigma Aldrich), 1,3-dioxolane (DOL, 99.8%, Sigma Aldrich), Dimethyl

trisulfide (DMTS, CH_3SSSCH_3, 98%, 1.19 g/mL, Acros Organics), Dimethyl disulfide (DMDS, CH_3SSCH_3, 99%, Acros Organics), sulfur (99.5%, Alfa Aesar) and lithium sulfide (Li_2S, 99.98%, Sigma Aldrich)were purchased and used as received.

3.2.2 Preparation of MWCNT Paper

180 mg MWCNT (Nanostructure and Amorphous Materials, Inc.) were dispersed in a miscible solution of de-ionized water (500 mL) and isopropyl alcohol (20 mL) by ultrasonication for 15 min, followed by vacuum filtration to render a free-standing MWCNT paper. The MWCNT paper was dried in an air-oven for 24 h at 100 °C before being peeled off and punched out into circular disks with 1.11 cm diameter (0.97 cm^2 in area, 4.5-4.9 mg in mass) for use as the current collector.

3.2.3 Electrolyte and DMTS Catholyte Preparation

The regular electrolyte was composed of 1 M lithium bis(trifluoromethanesulfonyl) imide (LiTFSI) and 0.1 M $LiNO_3$ in 1, 2-dimethoxyethane (DME) and 1,3-dioxolane (DOL) (v/v, 1:1). The DMTS catholyte were prepared by adding DMTS to the regular electrolyte. The volume ratio of DMTS to the regular electrolyte were 1:4, and 1:2, respectively. Because DMTS is miscible with ethers, no phase separation was found.

3.2.4 DMTS Cell Fabrication

First, DMTS catholyte (28 μL) was added into the MWCNT paper electrode, corresponding to 6.5 mg (6.7 mg cm^{-2}), and 11.0 mg (11.3 mg cm^{-2}) of DMTS calculated by the catholyte mass and DMTS mass percent, respectively, for the two different DMTS catholytes. Then a Celgard 2400 separator was placed on the top of the MWCNT paper electrode followed by adding 15 μL regular electrolyte on the top side of separator. Finally, lithium metal anode was placed on the separator and as-

semble the cell. To avoid electrolyte evaporation, the liquid electrolyte and catholyte were quickly and carefully added onto the cathode and anode using a microsyringe.

3.2.5 Lithium Polysulfide Cell Fabrication

The lithium polysulfide/MWCNT paper electrode is prepared as follows: First, stoichiometric amounts of sulfur powder and Li_2S were mixed in anhydrous ethanol by magnetic stirring overnight at room temperature to render a 0.75 M Li_2S_6 (4.5 M sulfur) solution. 25 μL Li_2S_6 solution was added into the MWCNT paper, and dried in the glove box. Then another 25 μL Li_2S_6 was added, and the Li_2S_6/MWCNT was dried again. The corresponding sulfur content was calculated to be 7.2 mg (7.4 mg cm^{-2}). After the electrode was totally dried, 30 μL regular electrolyte was added on the Li_2S_6/MWCNT cathode, then a Celgard 2400 separator was placed on the top of the MWCNT paper electrode followed by adding 20 μL regular electrolyte on the top side of separator. Finally, lithium metal anode was placed on the separator and crimped the cell. To improve the cycling performance and coulombic efficiency, the regular electrolyte contains 0.1 M $LiNO_3$. The capacity is based on $1C = 1672\ mA\ g^{-1}$. The lithium/Li_2S_6 was first charged to 2.8 V at C/10 rate, and then cycled at 1.8-2.8 V at C/10 rate.

3.2.6 Characterizations

The X-ray diffraction (XRD) data of the discharged and recharged DMTS electrode were collected on a Bruker D8 Discover XRD Instrument equipped with Cu Kα radiation. The samples were protected in the sample holder with Kapton film. The scanning rate was 2° min^{-1}, and 2θ was set between 15° and 80°. The XRD pattern of the discharged DMDS electrode was also collected for comparison. The morphological characterizations of the cycled DMTS electrodes were conducted with a JEOL JSM-7800F field emission scanning electron microscopy (SEM). The elemental

mapping was performed with energy-dispersive X-ray spectroscopy (EDX) attached to the SEM with 15 KV.

X-ray Photoelectron Spectroscopy (XPS) measurements was performed on the PHI Versa Prove II instrument equipped with monochromatic Al Kα (1486.6 eV) radiation. The measurements were done with a detection angle of 45°, using pass energies at the analyzer of 93.9 and 29.35 eV for survey and detail spectra, respectively. For binding energy calibration the C (1s) peak was set to 284.8 eV. The sample surfaces were sputtered for 30 minutes (5 kV, 1 μA) for subsurface analysis.

GC-MS were analyzed with an Agilent 7890A gas chromatograph coupled to an Agilent 5975C mass spectrometer. Prior to each use, a 65 μM carboxen/polydimethylsiloxane (CAR/PDMS) solid phase micro-extraction (SPME) fiber (Supelco, USA) was prepared by insertion into the inlet at a temperature of 300 °C for 15 min with the oven at 200 °C. This process was utilized to remove impurities from the fiber and the column, and was verified by blank run. Next, the pure DMTS material was placed inside a 20 mL headspace vial inside a glove box and allowed to equilibrate for at least 1 h at room temperature. The headspace was then sampled at room temperature for 15 min by a freshly prepared PDMS/DVB SPME fiber prior to manual injection. The column is an Agilent J&W HP-5ms Ultira Inert GC Column, with the following specifications: 30 m column length, 0.25 mm internal diameter, 0.25 μm film thickness. The inlet was held at 250°C with a split flow of 1.024 mL /min (He carrier gas) and a split ratio of 100:1. The oven temperature program utilized an initial temperature of 40°C held for 2 minutes, followed by a ramp of 8 °C min^{-1} to 100 °C, 15 °C min^{-1} to 120 °C, 8 °C min^{-1} to 180 °C, 15 °C min^{-1} to 200 °C, and 8 °C min^{-1} to 280 °C. The MS transfer line temperature was 250 °C. The mass spectrometer utilized an electron impact detector with a 3.20 min solvent delay and a scan range of m/z 26-250. The relevant components of each sample were identified based on the mass spectra in the National Institute of Standards and Technology (NIST) version 08 mass spectral database. The discharged DMTS electrode, and recharged DMTS electrode were identified with the same procedure.

3.3 Results and Discussion

DMTS has a high theoretical capacity of 849 mAh g^{-1} considering a $4e^-$ reduction reaction, and the possible cathodic reaction is illustrated in Figure 3.1a. In the lithiation step, the DMTS could gain $4Li^+$ and $4e^-$ to form two lithium thiomethoxide ($LiSCH_3$) and one Li_2S. In the delithiation step, these discharge products would be converted back to DMTS. DMTS is a liquid at room temperature and can be miscible with the ether-based electrolyte. Inspired by our previous work on Li/dissolved polysulfide batteries, binder-free multiwalled carbon nanotube (MWCNT) paper was used as the current collector and liquid reservoir [48, 84]. $LiNO_3$ was added in the catholyte and electrolyte to passivate the lithium metal anode and improve cycling stability. A cutoff voltage at 1.7 V is used in the cycling performance measurement because $LiNO_3$ could be reduced at lower voltage [85, 86] The DMTS catholyte contains 19.2 - 32.2% weight percent of DMTS in the ether-based electrolyte composed of 1 M LiTFSI and 0.1 M $LiNO_3$ in 1,2-dimethoxyethane (DME) and 1,3-dioxolane (DOL) (1:1, v:v). 28 μL of DMTS catholyte was injected into the MWCNT paper on the cathode side, then another 15 μL blank electrolyte was added to the lithium metal anode side, the open circuit voltage of the cell is about 2.4 V. Cyclic voltammetry (CV) was performed on a BioLogic VSP potentiostat from open circuit voltage to 1.7 V, and then recharged back to 2.7 V at a scanning rate of 20 μV s^{-1}. Cells were galvanostatically cycled on an Arbin BT2000 battery tester at current densities mentioned in the discussion from 1.7 to 2.7 V. The current rates and specific capacities were based on the mass of DMTS present in the cathode (1C = 849 mA g^{-1}).

The cell was discharged first and cycled between 1.7 - 2.7 V at C/10 rate. The voltage profile shown in Figure 3.1c demonstrates the DMTS is electrochemically reversible, and the first discharge curve consists of three regions: 1) a short slope in the beginning of discharge (almost 18% of the discharge capacity), 2) a linear voltage plateau at 2.06 V, and 3) a relative longer voltage slope range from 2 to 1.7 V. The first discharge time is about 8.5 h corresponding to 85% of the theoretical discharge

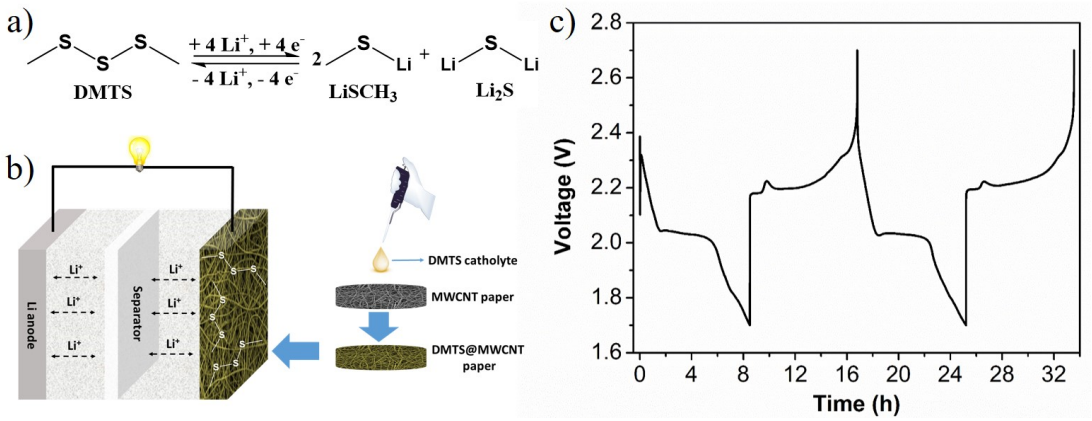

Figure 3.1. a) The possible redox reaction of DMTS; b) Schematic illustration of the cell configuration and the addition of DMTS catholyte into MWCNT paper electrode; c) The voltage-time profile of the cell with $LiNO_3$ containing ether electrolyte cycled between 1.7 - 2.7 V at C/10 rate.

time of DMTS when the cutoff voltage is 1.7 V. The charge process consists of a voltage plateau at about 2.2 V in the first half followed by gradual increase in the second half. The discharge time and charge time are almost equal, meaning a high Coulombic efficiency. The second cycle shows a same voltage profile as the first one. The cyclic voltammogram (CV) profile of the cell shown in Figure 3.2 reflects the voltage profile in Figure 3.1c.

To disclose the reaction mechanism of DMTS in the discharge and charge processes, X-ray diffraction (XRD) was first conducted to identify the cycled products of DMTS. All samples have been washed by DME completely to remove all soluble species before the measurements. Considering no XRD pattern of $LiSCH_3$ was reported in literature, the discharged product of DMDS, which should be $LiSCH_3$ according to the disulfide/thiolate redox reaction mechanism [87], was used as a reference. As displayed in Figure 3.3a, nearly all the peaks for the discharge products of DMTS match very well with those of DMDS, indicating $LiSCH_3$ is a primary discharged product of DMTS. For the recharged electrode, there is only one strong peak centered at around 26.0° belonging to the (002) plane of MWCNTs [88], showing all the charged products are oxidized to soluble species and washed away. This can be

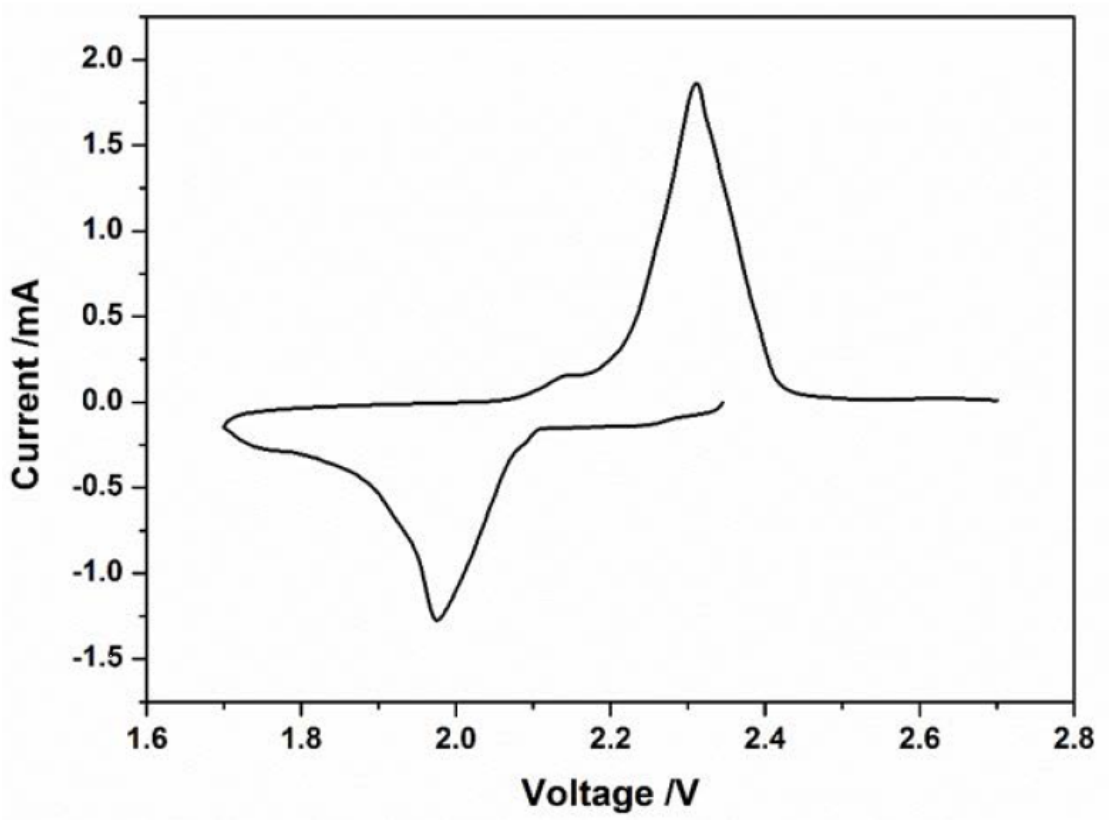

Figure 3.2. Cyclic voltammogram of the DMTS catholyte cycling between 1.7 - 2.7 V at a voltage scanning rate of 0.02 mV s^{-1}.

further confirmed by the SEM and EDS analysis of the washed, recharged electrode of DMTS, as shown in Figure 3.3b. The recharged electrode shows a clean MWCNT network which is similar to the pristine MWCNT paper shown in Figure 3.9a.

X-ray photoelectron spectroscopy (XPS) was conducted to identify the sulfur species in the discharged electrode of DMTS. Figure 3.3c shows the XPS spectra of a discharged electrode at 1.7 V (I) and another discharged electrode at 1.0 V (II), and commercial Li_2S sample (III) as a reference. The commercial Li_2S shows the S $2p_{3/2}$ peak centered at 160.9 eV and S $2p_{1/2}$ peak centered at 162.1 eV. The first discharged sample shows three different S $2p_{3/2}$ peaks at 164.0, 162.4, and 160.9 eV, indicating three different types of sulfur compounds. The S $2p_{3/2}$ peak centers at 160.9 eV is attributed to the Li_2S, confirming lithium sulfide is a discharged product

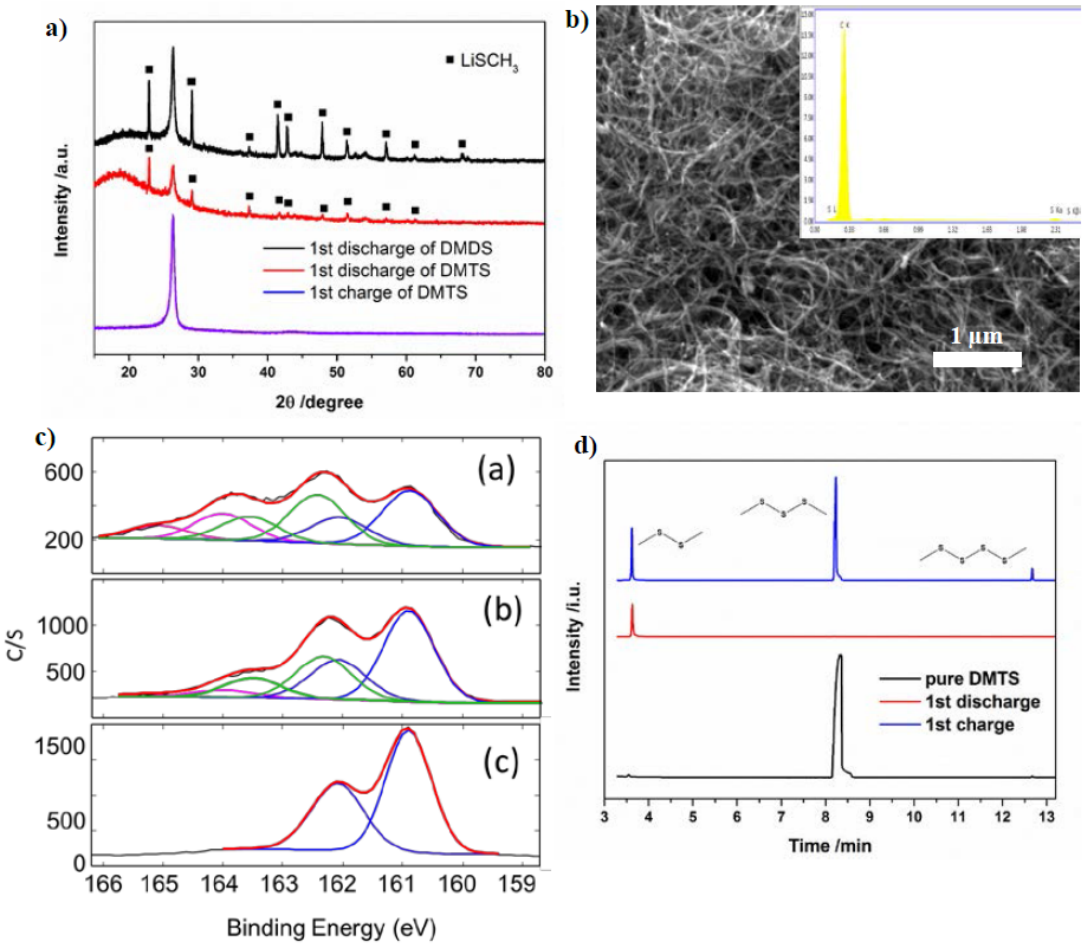

Figure 3.3. a) XRD pattern of the discharged electrode of DMDS, the discharged and recharged electrode of DMTS; b) SEM image of the surface of the recharged electrode of DMTS after washed by DME, the inset image is the EDS analysis; c) XPS analysis of the incomplete discharged (a), and complete discharged DMTS (b), and the commercial Li_2S (c); d) GC-MS spectra of pure DMTS, the incomplete discharged electrode, and recharged electrode of DMTS.

of DMTS. Although the four main peaks of Li_2S (111, 200, 220, 311) are not seen in the XRD pattern in Figure 3.3a, it can be concluded here that the formed Li_2S is in an amorphous state [9, 48]. According to the recent literature [89], the S $2p_{3/2}$ peak locates at around 162.4 and 164.0 eV are attributed to $LiSCH_3$ and $LiSSCH_3$, respectively. The XPS pattern for the second discharged sample of DMTS only displays two main S $2p_{3/2}$ peaks centered at 160.9 and 162.4 eV, which can be only ascribed to Li_2S and $LiSCH_3$, respectively. This comparison indicates that $LiSSCH_3$

is an incomplete discharged product of DMTS if the cutoff voltage is ≥1.7 V and the discharged products are almost completely Li_2S and $LiSCH_3$ if the cutoff voltage is 1.0 V. According to the cell reaction described in Figure 3.1a, the sulfur peak area ratio in $LiSCH_3$ and Li_2S should be 2:1, however, this ratio is far less than 2:1 in Figure 3.3c, which could be due to partial solubility of $LiSCH_3$ in DME.

To identify the charged products of DMTS, we turned to gas chromatography-mass spectrometry (GC-MS). A carbon fiber probe was used to collect the vapor of these samples to avoid the salt contamination on the instrument. Pristine DMTS shows a strong peak at the retention time of 8.4 min in GC in Figure 3.3d and the highest mass/charge ratio (m/z) = 126 shown in MS in Figure 3.4 can be attributed to DMTS. The discharged sample which was collected at 1.7 V only shows a small peak at 3.6 min. The m/z = 94 confirms the vapor product is DMDS. The recharged sample, however, shows three peaks at 3.6, 8.4, and 12.6 min, corresponding to DMDS, DMTS, and dimethyl tetrasulfide (DMTtS), respectively, based on m/z ratios in Figure 3.4. Two negligible peaks at 3.6 and 12.6 min are also seen in the DMTS sample, meaning the starting material contains impurities of DMDS and DMTtS.

From the analysis of XRD, SEM, XPS, and GC-MS, we can formulate the cell reactions. The discharge and charge processes of DMTS can be described as follow. The primary discharged products are $LiSCH_3$ and Li_2S, which confirm the reaction in Figure 3.1a is true. In the incomplete discharge process with a high cutoff voltage, i.e., 1.7 V, small amounts of $LiSSCH_3$ and DMDS are present. The primary recharged product is the starting material, i.e., DMTS. Some DMDS and DMTtS co-exist in the recharged products.

The discharge process of DMTS can be separated into two steps. In the 1st discharge step involving $2e^-$, the S-S bonds in DMTS could break to form two radicals ($\cdot SCH_3$ and $\cdot SSCH_3$), which could react with Li^+ and e^- to form thiolates, i.e., $LiSCH_3$ and $LiSSCH_3$, or re-form S-S bonds to form shorter-chain DMDS or longer-chain DMTtS, as shown in the following. The geometry of the HOMO (3p orbital) of the sulfur atoms in $\cdot SCH_3$ and $\cdot SSCH_3$ are symmetric with that of the LUMO (2s orbital)

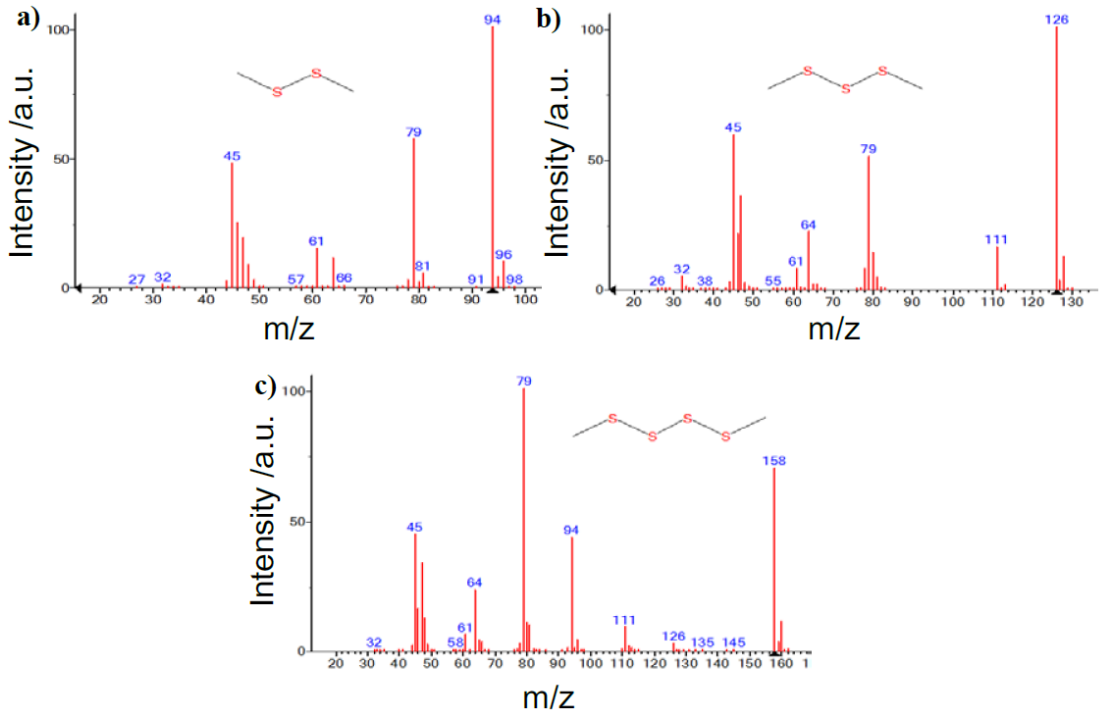

Figure 3.4. Mass spectra of a) dimethyl disulfide; b) dimethyl trisulfide; c) dimethyl tetrasulfide.

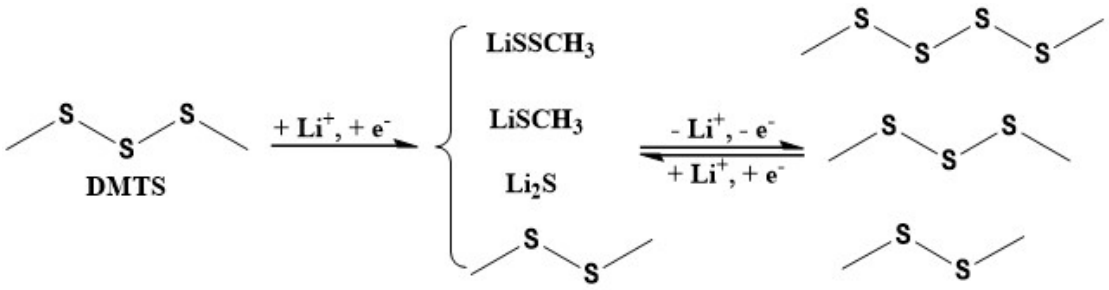

of Li^+, and their orbital potential energies (-11.62 eV for S and -5.39 eV for Li^+) are close to each other ($\Delta E < 12\ eV$), indicating the $\cdot SCH_3$ and $\cdot SSCH_3$ could easily react with Li^+ and $1e^-$ to form $LiSCH_3$ and $LiSSCH_3$, as expressed in Figure 3.5. Although the ·S radicals themselves can react with each other to form DMDS or DMTtS, considering the very large number of Li^+ in the electrolyte and the small radius of Li^+, it is reasonable to believe the cell reaction 1 to be the main reaction and the cell reactions 2 and 3 are minor. The formed small amount of DMTtS would

soon get reduced and cannot be detected by GC-MS because the dissociation energy of the S-S bond in DMTtS is even lower than that in DMTS [82].

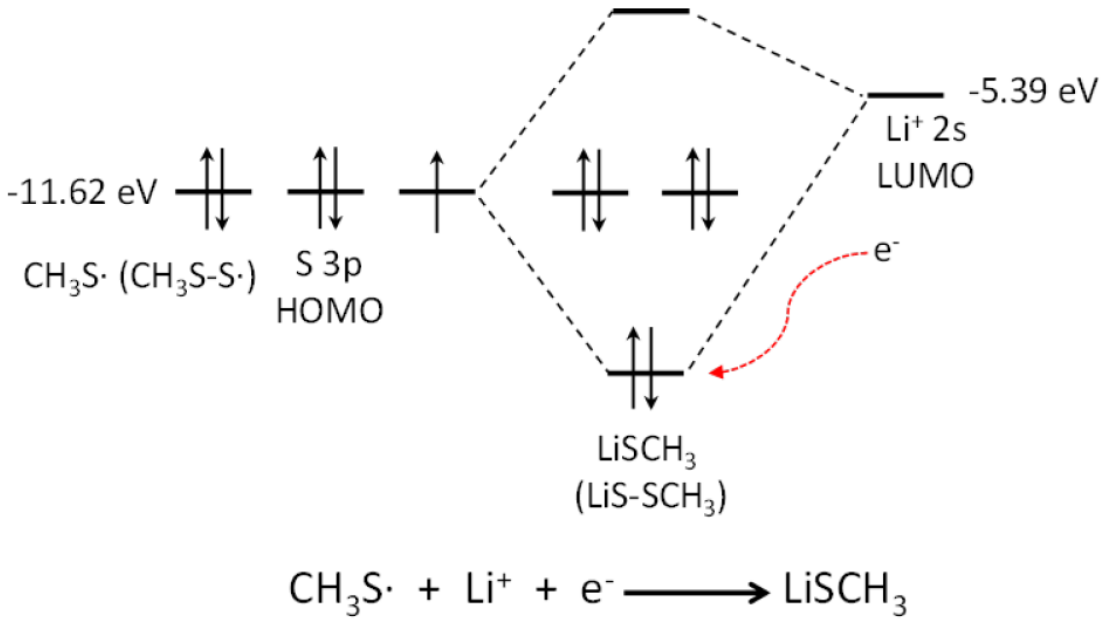

Figure 3.5. The reaction of CH_3S radical, lithium cation, electron, and its corresponding molecular orbital.

Reaction 1:	$CH_3SSSCH_3 \xrightarrow{+2Li^+, +2e} LiSCH_3 + LiSSCH_3$		Main
Reaction 2:	$2\,CH_3SSSCH_3 \xrightarrow{+2Li^+, +2e} CH_3SSCH_3 + 2\,LiSSCH_3$		minor
Reaction 3:	$2\,CH_3SSSCH_3 \xrightarrow{+2Li^+, +2e} 2\,LiSCH_3 + CH_3SSSSCH_3$		minor

The formed DMDS is reduced in the 2^{nd} discharge step involving $2e^-$. The main reaction of this step is the reduction of $LiSSCH_3$ to form Li_2S and $LiSCH_3$. In this step, the $\cdot SCH_3$ radicals are formed again and two of them could be combined to form DMDS which is detected in GC-MS. Similarly, due to the large number of Li^+ ions, the reaction 4 would be the main reaction, the reaction 5 would be minor and a small amount of DMDS is formed again. Owing to the similarity of S-S bonds in $LiSSCH_3$,

LiSSSLi, and LiSSLi, the reduction of $LiSSCH_3$ leads to the main voltage plateau at around 2.06 V in the discharge.

Reaction 4: $LiSSCH_3 \xrightarrow{+2Li^+, +2e} Li_2S + LiSCH_3$ Main

Reaction 5: $2\,LiSSCH_3 \xrightarrow{+2Li^+, +2e} 2\,Li_2S + CH_3SSCH_3$ minor

In the recharge step, Li_2S and all these thiolates are de-lithiated. The radicals of $\cdot SCH_3$ and $\cdot SSCH_3$ are formed again and they can form DMDS, DMTS, and DMTtS which are all detected in GC-MS. The de-lithiation requires higher energy than the lithiation, resulting in higher charge voltage than the discharge voltage, as shown in Figure 3.1c.

The battery performance of DMTS was measured. A DMTS catholyte was used in the cell with high loading of 6.7 mg cm^{-2} DMTS in the cathode. Figure 3.6a presents the extended cycling performance and Coulombic efficiency of the cell cycled between 1.7 - 2.7 V at C/10 rate (1C = 849 mAh g^{-1}). The initial discharge capacity is up to 720 mAh g^{-1}, which equals to 85% of the theoretical capacity. After 70 cycles, the discharge capacity is still as high as 527 mAh g^{-1}, retaining 73% of the initial capacity. The Coulombic efficiency is up to 98% for most cycles. The corresponding voltage-capacity profiles are displayed in Figure 3.6b. Overall, the voltage-capacity curves of different cycles are similar. In the discharge, they all have a small high-voltage region between 2.3 - 2.1 V in the beginning, a long constant plateau at around 2 V in the middle, and a decreasing voltage slope at the end. The 2 V plateau decreases from 53% to 41% after 70 cycles, which is due to the continuous content change of DMDS, DMTS, and DMTtS upon cycling. In addition, the 2 V voltage decreases as cycles, which is due to the increased impedance resulting from the of the tarnished lithium anode. In the recharge, they all have a long voltage plateau at around 2.2 V followed by an increasing voltage slope.

The rate performance of a cell with the DMTS catholyte is shown in Figure 3.6c. The cell shows discharge capacities of about 658, 582, 462, and 317 mAh g^{-1} at C/10,

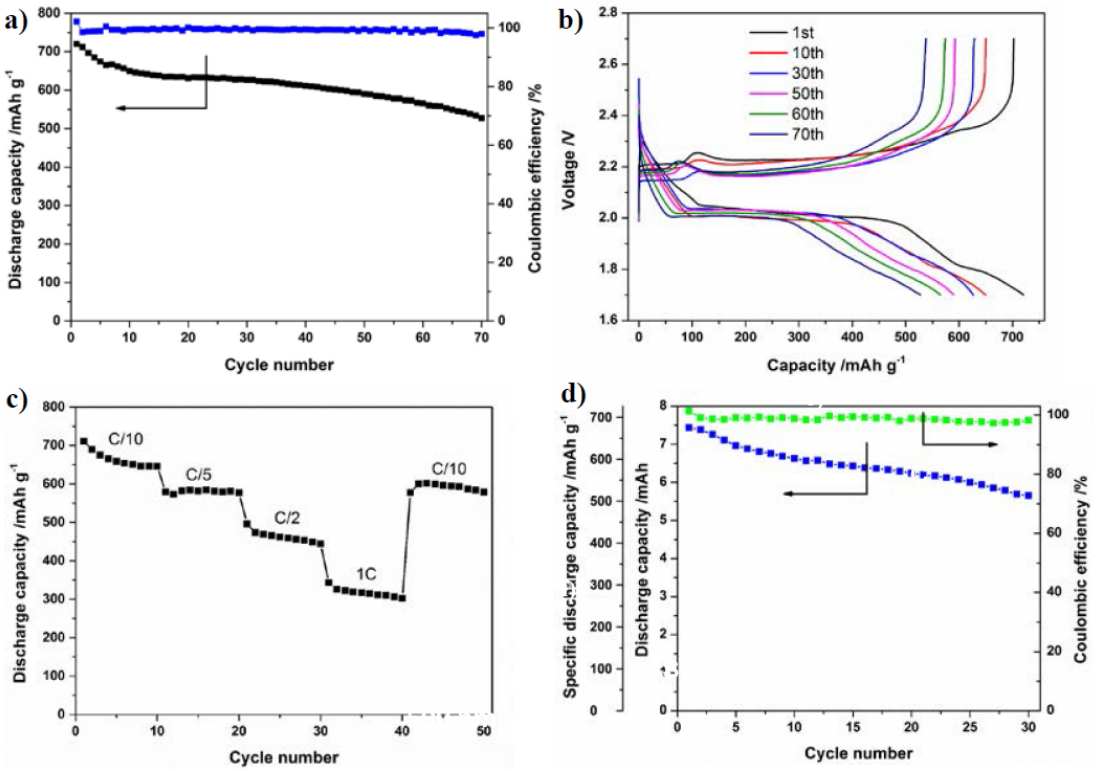

Figure 3.6. a) The cycling performance and Coulombic efficiency of a cell cycled between 1.7 - 2.7 V at C/10 rate; b) The corresponding voltage-capacity profile after different cycles; c) Rate performance of a cell cycled at C/10, C/5, C/2, and 1C rates; d) The cyclability and Coulombic efficiency of a cell cycled between 1.7 - 2.7 V at C/10 rate with DMTS loading of 11.3 mg cm^{-2}.

C/5, C/2, and 1C, respectively. At each rate, the discharge capacity slowly decreases as cycles. When the rate regained to C/10, the discharge capacity recovered to 597 mAh g^{-1}. After cycled for 50 cycles, the discharge capacity is 580 mAh g^{-1}, which retains 81% of the initial capacity at C/10 rate. The corresponding representative voltage profile at different rates is shown in Figure 3.7. It can be seen that the charge/discharge voltage difference in the middle of each process increases from 0.15 V to 0.58 V as the rate increases from C/10 to 1C.

In order to demonstrate a high energy density battery with DMTS cathode, we further increased the DMTS weight ratio in the catholyte (DMTS: DME: DOL = 1:1:1 v/v/v). For the cathode side, we used 28 μL catholyte, corresponding to DMTS

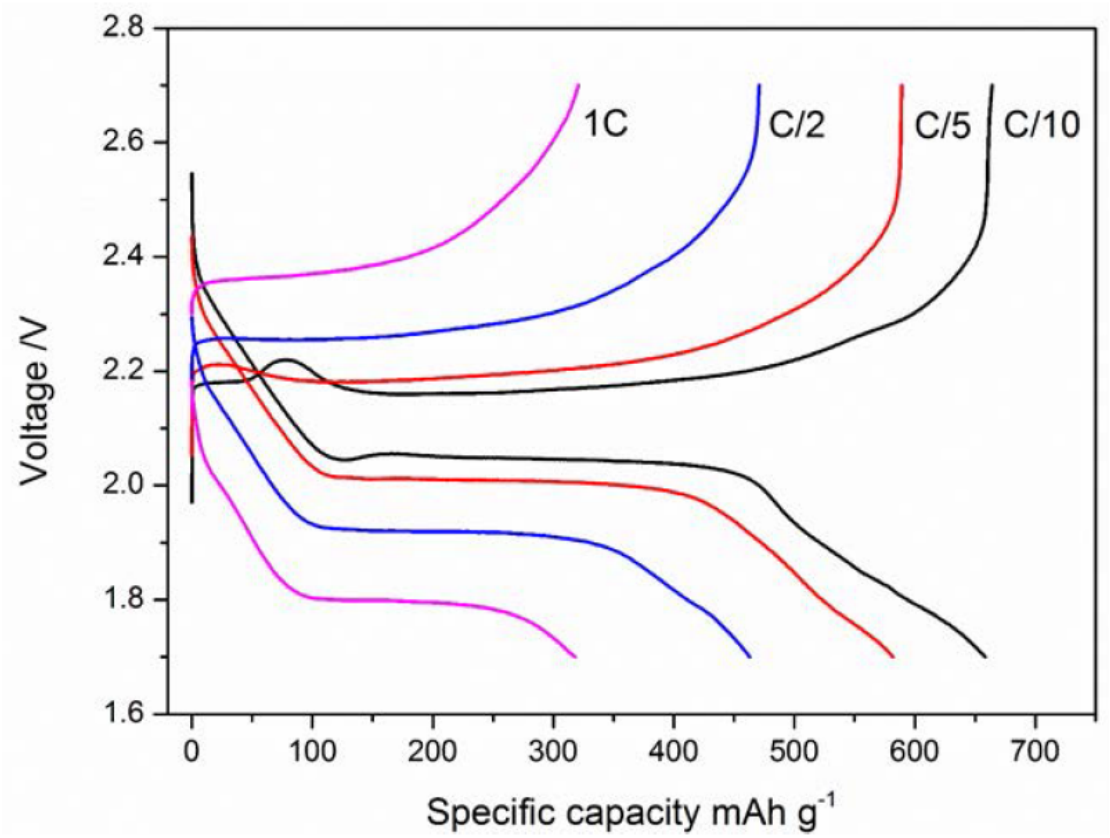

Figure 3.7. Typical voltage versus specific capacity profiles of DMTS cell at different rates.

loading of 11.3 mg cm^{-2} and an electrolyte/DMTS ratio of 3:1 mL g^{-1}. Figure 3.6d shows its cycling performance at C/10 rate. The initial discharge capacity is up to 7.42 mAh, corresponding to a specific discharge capacity of 675 mAh g^{-1}. After 30 cycles, the cell discharge capacity is still as high as 5.67 mAh. The Coulombic efficiency is above 98% for all 30 cycles. For comparison, we made a high-areal-capacity Li/polysulfide cell with the same MWCNT paper, the sulfur loading is 7.4 mg cm^{-2}, and the electrolyte we used is 50 μL in total, the electrolyte: sulfur ratio is controlled to be 6.9:1 (mL g^{-1}). Its cycling performance at C/10 rate is shown in Figure 3.8. The initial discharge capacity is 6.70 mAh, however the cell cannot be cycled anymore after 24 cycles, as shown in Figure 3.8b. The discharge capacity decreases to 4.11 mAh and the Coulombic efficiency decreases to 64.4%. To achieve a

real high energy density battery, it is vital to decrease the amount of electrolyte. For Li-S batteries, the optimal electrolyte/sulfur ratio is no less than 10 mL g^{-1}, which is too high to achieve a real energy battery [90, 91].

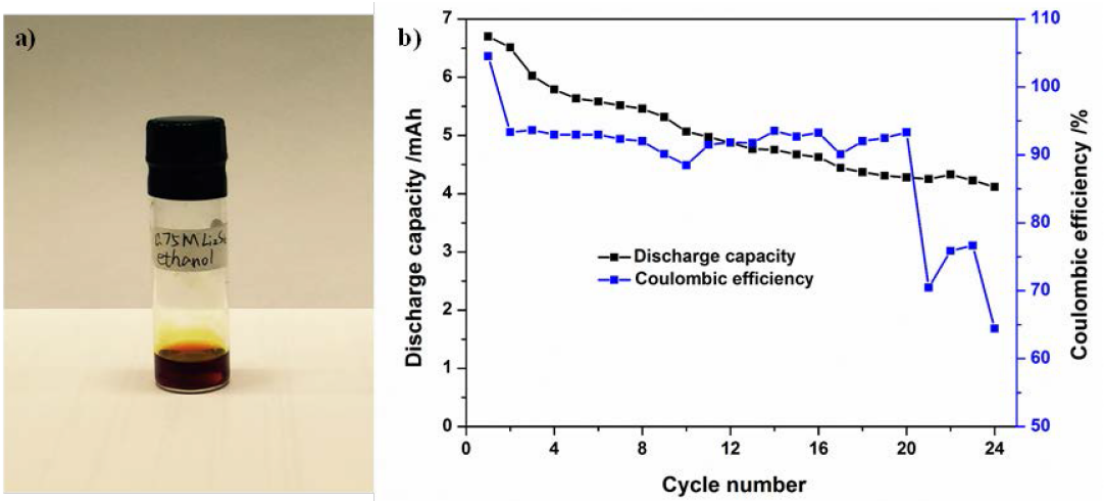

Figure 3.8. a) The photograph of 0.75 M Li_2S_6 solution (4.5 M sulfur) in anhydrous ethanol; b) the cycling performance and coulombic efficiency of the high loading Li-S batteries at C/10 rate.

Scanning electron microscopy (SEM) characterization was conducted to investigate the morphology of the discharged electrode after 70 cycles, as shown in Figure 3.9 (b-d). For comparison, the SEM image of the pristine MWCNT paper is shown in Figure 3.9a. Obviously, the MWCNTs still maintain a self-weaving, nanoporous network in the discharged electrode. And the nanopores are filled and all MWCNTs are coated with the discharged products. The elemental mapping of carbon (Figure 3.9e) and sulfur (3.9f) evidently validate the discharged products, i.e., $LiSCH_3$ and Li_2S, are homogeneous distributed in the cycled DMTS electrode.

The theoretical specific energies of some rechargeable lithium batteries and the Li/DMTS battery are shown in Figure 3.10a. The specific energy the Li/DMTS battery is calculated based on the theoretical capacities of DMTS (849 mAh g^{-1}) and lithium (3862 mAh g^{-1}), and cell voltage of 2.0 V. It is obvious that the Li/DMTS battery has a high specific energy of 1391 Wh kg^{-1}, which is 3.6 times that of the con-

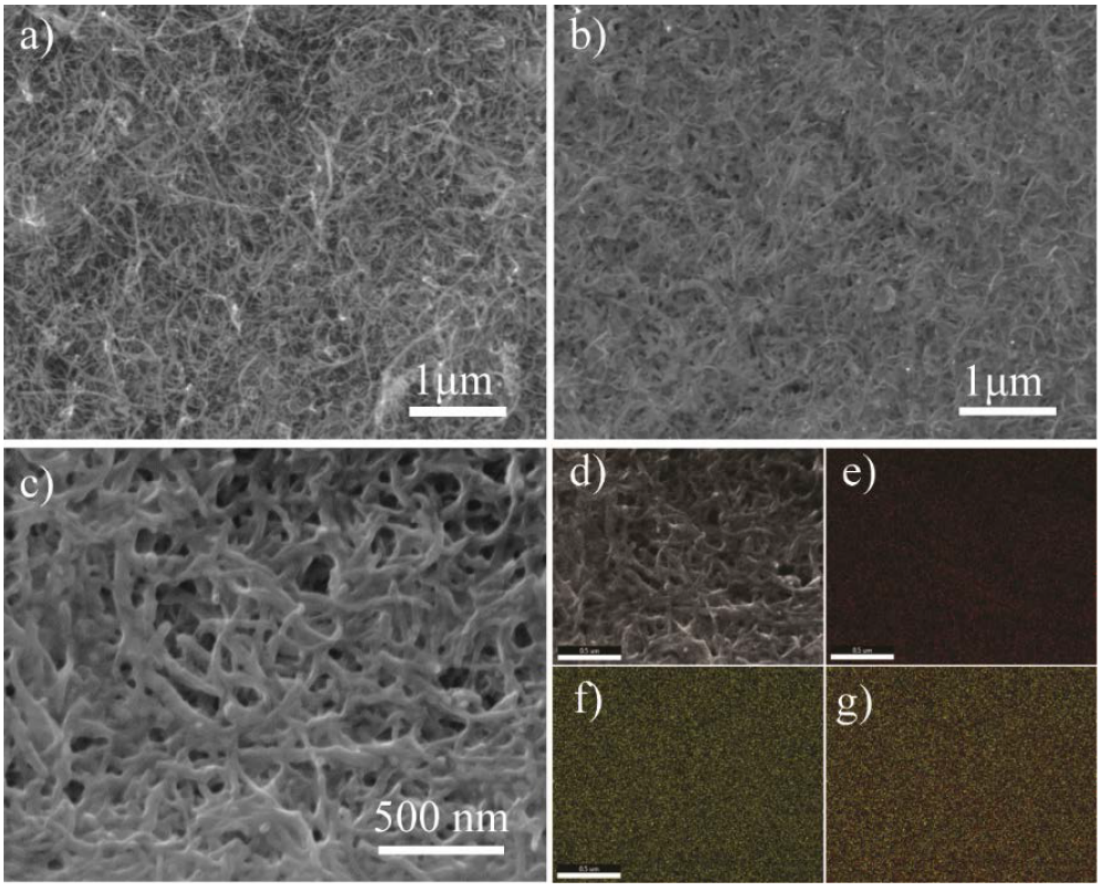

Figure 3.9. SEM image of the surface morphology of a) pristine MWCNT paper; b-d) Discharged electrode of after 70 cycles; Elemental mapping of e) carbon; f) sulfur; g) overlapped carbon and sulfur.

ventional Li-ion batteries, 2.4 and 2.5 times those of the lithium-iodine and lithium-anthraquinone batteries, respectively. The experimental specific energies in terms of electrodes (lithium and DMTS) and the cell (electrodes and electrolyte) are displayed in Figure 3.10b. Representative data are collected after 5 cycles. When the electrolyte/DMTS ratio equals to 5.7:1 (mL g^{-1}), the specific energy is 1106 Wh kg^{-1} for the electrodes alone, and the specific energy is 147 Wh kg^{-1} for the cell. When the electrolyte/DMTS ratio decreases to 3:1 (mL g^{-1}), the specific energy for the electrodes decreases to 1025 Wh kg^{-1}, however the specific energy for the cell increases to 229 Wh kg^{-1}. To the best of our knowledge, these specific energies are the

highest records among organic cathode materials. More importantly, the cell specific energy is even higher than those of the most reported Li-S batteries as the high electrolyte/sulfur mass ratio ($\geq$10:1) limiting the specific energy of Li-S batteries [90–95].

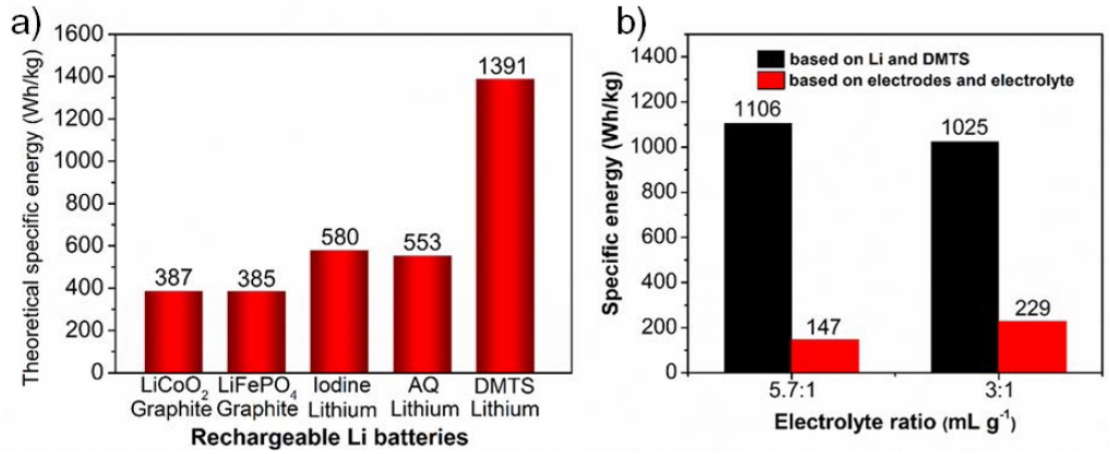

Figure 3.10. a) Comparison of theoretical specific energy of some rechargeable lithium batteries ($LiCoO_2$/graphite [2], $LiFePO_4$/graphite [5], Li-I_2 [96], Li/anthraquinone [15]) with the Li/DMTS battery; b) The specific energies two cells with different electrolyte/DMTS ratios after five cycles, the specific energy density is calculated based on either the mass of lithium and DMTS or the mass of electrodes and electrolyte.

3.4 Conclusions

We have demonstrated that dimethyl trisulfide is a high capacity and high specific energy organosulfide cathode material for rechargeable lithium batteries. The XRD and XPS analysis on the first discharged electrodes indicates the reduction is almost a $4e^-$ reduction process and the discharge products are mostly $LiSCH_3$ and Li_2S. The GC-MS results confirm the recharged products consist of DMDS, DMTS, and DMTtS, representing a complicated electrochemical process. Using an ether-based electrolyte with $LiNO_3$ additive, DMTS can be cycled in the form of a catholyte in a binder-free carbon nanotube current collector. The cell delivers an initial discharge capacity of 720 mAh g^{-1} and retains 74% of the initial capacity over 70 cycles with high DMTS

loading of 6.7 mg cm^{-2} at C/10 rate. When the DMTS loading is increased to 11.3 mg cm^{-2}, the specific energy is 1025 Wh kg^{-1} for the active materials alone including lithium and the specific energy is 229 Wh kg^{-1} for the cell including electrolyte. Variations on the organic group R in the organotrisulfide can be made to enable a new class of high capacity cathode materials for high energy rechargeable lithium batteries.

4. CONCLUSIONS

4.1 Li_2S Cathode

Lithium sulfide (Li_2S) with a high theoretical capacity of 1166 mAh g^{-1} is a promising cathode material for Li-S batteries as it allows for the use of lithium-free anodes. However, a large overpotential ($\sim$1 V) is usually needed to activate microsized Li_2S particles due to their low electronic and ionic conductivities. Here, nano-Li_2S/carbon paper electrodes are developed via a simple Li_2S solution filtration method. Li_2S nanocrystals with a size less than 10 nm are formed uniformly in the pores of carbon paper network. These electrodes show an unprecedented low potential difference (0.1 V) in the first and following charges, also show high discharge capacities, good rate capability, and excellent cycling performance. More specifically, the nano-Li_2S/carbon nanotube paper electrodes show a reversible capacity of 634 mAh g^{-1} with a capacity retention of 92.4% at 1C rate from the 4th to 100th cycle, corresponding to a low capacity fading rate of 0.078% per cycle. These results demonstrate a facile and scalable electrode fabrication process for making high performance nano-Li_2S/carbon paper electrodes, and the superior performance makes them promising for use with lithium metal-free anodes in rechargeable Li-S batteries for practical applications.

4.2 Organotrisulfide Cathode

The electrochemical active organic materials are promising electrode materials for rechargeable Li/Na batteries, supercapacitors, thin-film batteries, and redox flow batteries because of their unique traits like structural diversity, solubility, and flexibility. Organodisulfide materials are a group of organic electrode materials and have been investigated intensively. Compared to organodisulfides, the organotrisulfides have

higher capacity and faster kinetics due to the extra middle sulfur atom. We have demonstrated a small organotrisulfide compound, e.g. dimethyl trisulfide, to be a high capacity and high specific energy organosulfide cathode material for rechargeable lithium batteries. Based on XRD, XPS, SEM, and GC-MS analysis, we investigated its cell reaction mechanism. The redox reaction of DMTS is a $4e^-$ process and the main discharge products are $LiSCH_3$ and Li_2S. But after 1 cycle, the cell reaction become quite complicated, apart from the major product of DMTS, the high order organic polysulfide DMTtS and low order organic polysulfide DMDS are also formed and charged/discharged in the following cycles. With an ether-based electrolyte with $LiNO_3$ additive, DMTS cell delivers an initial discharge capacity of 720 mAh g^{-1} and retains 74% of the initial capacity over 70 cycles with high DMTS loading of 6.7 mg cm^{-2} at C/10 rate. When the DMTS loading is increased to 11.3 mg cm^{-2}, the specific energy is 1025 Wh kg^{-1} for the active materials (DMTS and lithium) and the specific energy is 229 Wh kg^{-1} for the cell including electrolyte. Variations on the organic group R in the organotrisulfide can be made to achieve a group of high capacity cathode materials for rechargeable lithium batteries.

LIST OF REFERENCES

LIST OF REFERENCES

[1] M. Wu, J. Wang, Z. Wu, H. L. Xin, and D. Wang, "Synergistic enhancement of nitrogen and sulfur co-doped graphene with carbon nanosphere insertion for the electrocatalytic oxygen reduction reaction," *Journal of Materials Chemistry A*, vol. 3, no. 15, pp. 7727–7731, 2015.

[2] P. G. Bruce, S. A. Freunberger, L. J. Hardwick, and J.-M. Tarascon, "Li-O_2 and Li-S batteries with high energy storage," *Nature Materials*, vol. 11, no. 1, pp. 19–29, 2012.

[3] A. Manthiram, Y. Fu, S.-H. Chung, C. Zu, and Y.-S. Su, "Rechargeable lithium–sulfur batteries," *Chemical Reviews*, vol. 114, no. 23, pp. 11 751–11 787, 2014.

[4] J. B. Goodenough and Y. Kim, "Challenges for rechargeable Li batteries," *Chemistry of Materials*, vol. 22, no. 3, pp. 587–603, 2009.

[5] Y. Yang, M. T. McDowell, A. Jackson, J. J. Cha, S. S. Hong, and Y. Cui, "New nanostructured Li_2S/silicon rechargeable battery with high specific energy," *Nano Letters*, vol. 10, no. 4, pp. 1486–1491, 2010.

[6] S. Meini, R. Elazari, A. Rosenman, A. Garsuch, and D. Aurbach, "The use of redox mediators for enhancing utilization of Li_2S cathodes for advanced Li–S battery systems," *The journal of Physical Chemistry Letters*, vol. 5, no. 5, pp. 915–918, 2014.

[7] K. R. Ryan, L. Trahey, B. J. Ingram, and A. K. Burrell, "Limited stability of ether-based solvents in lithium–oxygen batteries," *The Journal of Physical Chemistry C*, vol. 116, no. 37, pp. 19 724–19 728, 2012.

[8] C. Zu, M. Klein, and A. Manthiram, "Activated Li_2S as a high-performance cathode for rechargeable Lithium–Sulfur batteries," *The Journal of Physical Chemistry Letters*, vol. 5, no. 22, pp. 3986–3991, 2014.

[9] Y. Fu, C. Zu, and A. Manthiram, "In situ-formed Li_2S in lithiated graphite electrodes for lithium–sulfur batteries," *Journal of the American Chemical Society*, vol. 135, no. 48, pp. 18 044–18 047, 2013.

[10] Y. Liang, Z. Tao, and J. Chen, "Organic electrode materials for rechargeable lithium batteries," *Advanced Energy Materials*, vol. 2, no. 7, pp. 742–769, 2012.

[11] Z. Song and H. Zhou, "Towards sustainable and versatile energy storage devices: an overview of organic electrode materials," *Energy & Environmental Science*, vol. 6, no. 8, pp. 2280–2301, 2013.

[12] N. Oyama, T. Tatsuma, T. Sato, and T. Sotomura, "Dimercaptan–polyaniline composite electrodes for lithium batteries with high energy density," vol. 373, pp. 598–600, 1995.

[13] J. Li, H. Zhan, and Y. Zhou, "Synthesis and electrochemical properties of polypyrrole-coated poly (2, 5-dimercapto-1, 3, 4-thiadiazole)," *Electrochemistry Communications*, vol. 5, no. 7, pp. 555–560, 2003.

[14] Z. Song, H. Zhan, and Y. Zhou, "Anthraquinone based polymer as high performance cathode material for rechargeable lithium batteries," *Chemical Communications*, no. 4, pp. 448–450, 2009.

[15] K. Zhang, C. Guo, Q. Zhao, Z. Niu, and J. Chen, "High-performance organic lithium batteries with an ether-based electrolyte and 9, 10-anthraquinone (AQ)/CMK-3 cathode," *Advanced Science*, vol. 2, no. 5, p. 1500018, 2015.

[16] Z. Song, Y. Qian, M. L. Gordin, D. Tang, T. Xu, M. Otani, H. Zhan, H. Zhou, and D. Wang, "Polyanthraquinone as a reliable organic electrode for stable and fast lithium storage," *Angewandte Chemie*, vol. 127, no. 47, pp. 14 153–14 157, 2015.

[17] G. A. Snook, P. Kao, and A. S. Best, "Conducting-polymer-based supercapacitor devices and electrodes," *Journal of Power Sources*, vol. 196, no. 1, pp. 1–12, 2011.

[18] F. R. Brushett, J. T. Vaughey, and A. N. Jansen, "An all-organic non-aqueous Lithium-Ion redox flow battery," *Advanced Energy Materials*, vol. 2, no. 11, pp. 1390–1396, 2012.

[19] Z. Song, Y. Qian, T. Zhang, M. Otani, and H. Zhou, "Poly (benzoquinonyl sulfide) as a high-energy organic cathode for rechargeable Li and Na batteries," *Advanced Science*, vol. 2, no. 9, p. 1500124, 2015.

[20] S. J. Visco and L. C. DeJonghe, "Ionic conductivity of organosulfur melts for advanced storage electrodes," *Journal of The Electrochemical Society*, vol. 135, no. 12, pp. 2905–2909, 1988.

[21] X. Ji and L. F. Nazar, "Advances in Li–S batteries," *Journal of Materials Chemistry*, vol. 20, no. 44, pp. 9821–9826, 2010.

[22] A. Manthiram, Y. Fu, and Y.-S. Su, "Challenges and prospects of lithium–sulfur batteries," *Accounts of Chemical Research*, vol. 46, no. 5, pp. 1125–1134, 2012.

[23] Y.-X. Yin, S. Xin, Y.-G. Guo, and L.-J. Wan, "Lithium–sulfur batteries: Electrochemistry, materials, and prospects," *Angewandte Chemie International Edition*, vol. 52, no. 50, pp. 13 186–13 200, 2013.

[24] F. Ding, W. Xu, G. L. Graff, J. Zhang, M. L. Sushko, X. Chen, Y. Shao, M. H. Engelhard, Z. Nie, J. Xiao *et al.*, "Dendrite-free lithium deposition via self-healing electrostatic shield mechanism," *Journal of the American Chemical Society*, vol. 135, no. 11, pp. 4450–4456, 2013.

[25] Z. W. Seh, Q. Zhang, W. Li, G. Zheng, H. Yao, and Y. Cui, "Stable cycling of lithium sulfide cathodes through strong affinity with a bifunctional binder," *Chemical Science*, vol. 4, no. 9, pp. 3673–3677, 2013.

[26] Z. W. Seh, H. Wang, P.-C. Hsu, Q. Zhang, W. Li, G. Zheng, H. Yao, and Y. Cui, "Facile synthesis of Li_2S–polypyrrole composite structures for high-performance Li_2S cathodes," *Energy & Environmental Science*, vol. 7, no. 2, pp. 672–676, 2014.

[27] Y. Son, J.-S. Lee, Y. Son, J.-H. Jang, and J. Cho, "Recent advances in Lithium Sulfide Cathode materials and their use in Lithium Sulfur batteries," *Advanced Energy Materials*, vol. 5, no. 16, p. 1500110, 2015.

[28] J. Hassoun and B. Scrosati, "A high-performance polymer tin sulfur lithium ion battery," *Angewandte Chemie International Edition*, vol. 49, no. 13, pp. 2371–2374, 2010.

[29] J. Hassoun, Y.-K. Sun, and B. Scrosati, "Rechargeable lithium sulfide electrode for a polymer tin/sulfur lithium-ion battery," *Journal of Power Sources*, vol. 196, no. 1, pp. 343–348, 2011.

[30] K. Cai, M.-K. Song, E. J. Cairns, and Y. Zhang, "Nanostructured Li_2S–C composites as cathode material for high-energy lithium/sulfur batteries," *Nano Letters*, vol. 12, no. 12, pp. 6474–6479, 2012.

[31] Z. Yang, J. Guo, S. K. Das, Y. Yu, Z. Zhou, H. D. Abruña, and L. A. Archer, "In situ synthesis of lithium sulfide–carbon composites as cathode materials for rechargeable lithium batteries," *Journal of Materials Chemistry A*, vol. 1, no. 4, pp. 1433–1440, 2013.

[32] S. Jeong, D. Bresser, D. Buchholz, M. Winter, and S. Passerini, "Carbon coated lithium sulfide particles for lithium battery cathodes," *Journal of Power Sources*, vol. 235, pp. 220–225, 2013.

[33] M. Agostini, J. Hassoun, J. Liu, M. Jeong, H. Nara, T. Momma, T. Osaka, Y.-K. Sun, and B. Scrosati, "A lithium-ion sulfur battery based on a carbon-coated lithium-sulfide cathode and an electrodeposited silicon-based anode," *ACS Applied Materials & Interfaces*, vol. 6, no. 14, pp. 10 924–10 928, 2014.

[34] Z. W. Seh, J. H. Yu, W. Li, P.-C. Hsu, H. Wang, Y. Sun, H. Yao, Q. Zhang, and Y. Cui, "Two-dimensional layered transition metal disulphides for effective encapsulation of high-capacity lithium sulphide cathodes," *Nature Communications*, vol. 5, p. 5017, 2014.

[35] X. Meng, D. J. Comstock, T. T. Fister, and J. W. Elam, "Vapor-phase atomic-controllable growth of amorphous Li_2S for high-performance lithium–sulfur batteries," *ACS Nano*, vol. 8, no. 10, pp. 10 963–10 972, 2014.

[36] L. Wang, Y. Wang, and Y. Xia, "A high performance lithium-ion sulfur battery based on a Li_2S cathode using a dual-phase electrolyte," *Energy & Environmental Science*, vol. 8, no. 5, pp. 1551–1558, 2015.

[37] Y. Yang, G. Zheng, S. Misra, J. Nelson, M. F. Toney, and Y. Cui, "High-capacity micrometer-sized Li_2S particles as cathode materials for advanced rechargeable lithium-ion batteries," *Journal of the American Chemical Society*, vol. 134, no. 37, pp. 15 387–15 394, 2012.

[38] Y. Fu, Y.-S. Su, and A. Manthiram, "Li_2S-Carbon sandwiched electrodes with superior performance for Lithium-Sulfur batteries," *Advanced Energy Materials*, vol. 4, no. 1, 2014.

[39] R. Xu, X. Zhang, C. Yu, Y. Ren, J. Li, and I. Belharouak, "Paving the way for using Li_2S batteries," *ChemSusChem*, vol. 7, no. 9, pp. 2457–2460, 2014.

[40] F. Wu, J. T. Lee, N. Nitta, H. Kim, O. Borodin, and G. Yushin, "Lithium iodide as a promising electrolyte additive for lithium–sulfur batteries: mechanisms of performance enhancement," *Advanced Materials*, vol. 27, no. 1, pp. 101–108, 2015.

[41] J. Guo, Z. Yang, Y. Yu, H. D. Abruna, and L. A. Archer, "Lithium–sulfur battery cathode enabled by lithium–nitrile interaction," *Journal of the American Chemical Society*, vol. 135, no. 2, pp. 763–767, 2012.

[42] K. Zhang, L. Wang, Z. Hu, F. Cheng, and J. Chen, "Ultrasmall Li_2S nanoparticles anchored in graphene nanosheets for high-energy lithium-ion batteries," *Scientific Reports*, vol. 4, pp. 6467–6474, 2014.

[43] C. Nan, Z. Lin, H. Liao, M.-K. Song, Y. Li, and E. J. Cairns, "Durable carbon-coated Li_2S core–shell spheres for high performance Lithium/Sulfur cells," *Journal of the American Chemical Society*, vol. 136, no. 12, pp. 4659–4663, 2014.

[44] F. Wu, H. Kim, A. Magasinski, J. T. Lee, H.-T. Lin, and G. Yushin, "Harnessing steric separation of freshly nucleated Li_2S nanoparticles for bottom-up assembly of high-performance cathodes for Lithium-Sulfur and Lithium-Ion batteries," *Advanced Energy Materials*, vol. 4, no. 11, pp. 1 400 196–1 400 203, 2014.

[45] L. Suo, Y. Zhu, F. Han, T. Gao, C. Luo, X. Fan, Y.-S. Hu, and C. Wang, "Carbon cage encapsulating nano-cluster Li_2S by ionic liquid polymerization and pyrolysis for high performance Li–S batteries," *Nano Energy*, vol. 13, pp. 467–473, 2015.

[46] F. Wu, A. Magasinski, and G. Yushin, "Nanoporous Li_2S and MWCNT-linked Li_2S powder cathodes for lithium-sulfur and lithium-ion battery chemistries," *Journal of Materials Chemistry A*, vol. 2, no. 17, pp. 6064–6070, 2014.

[47] C. Wang, X. Wang, Y. Yang, A. Kushima, J. Chen, Y. Huang, and J. Li, "Slurryless Li_2S/reduced graphene oxide cathode paper for high-performance lithium sulfur battery," *Nano Letters*, vol. 15, no. 3, pp. 1796–1802, 2015.

[48] Y. Fu, Y.-S. Su, and A. Manthiram, "Highly reversible lithium/dissolved polysulfide batteries with carbon nanotube electrodes," *Angewandte Chemie*, vol. 125, no. 27, pp. 7068–7073, 2013.

[49] F. Wu, J. T. Lee, A. Magasinski, H. Kim, and G. Yushin, "Solution-based processing of graphene–Li_2S composite cathodes for Lithium-Ion and Lithium–Sulfur batteries," *Particle & Particle Systems Characterization*, vol. 31, no. 6, pp. 639–644, 2014.

[50] A. Patterson, "The scherrer formula for X-ray particle size determination," *Physical Review*, vol. 56, no. 10, p. 978, 1939.

[51] U. Holzwarth and N. Gibson, "The Scherrer equation versus the 'Debye-Scherrer equation'," *Nature Nanotechnology*, vol. 6, no. 9, pp. 534–534, 2011.

[52] C. Barchasz, F. Molton, C. Duboc, J.-C. Leprêtre, S. Patoux, and F. Alloin, "Lithium/sulfur cell discharge mechanism: an original approach for intermediate species identification," *Analytical Chemistry*, vol. 84, no. 9, pp. 3973–3980, 2012.

[53] Z. Lin, C. Nan, Y. Ye, J. Guo, J. Zhu, and E. J. Cairns, "High-performance lithium/sulfur cells with a bi-functionally immobilized sulfur cathode," *Nano Energy*, vol. 9, pp. 408–416, 2014.

[54] J. Liu, H. Nara, T. Yokoshima, T. Momma, and T. Osaka, "Li_2S cathode modified with polyvinylpyrrolidone and mechanical milling with carbon," *Journal of Power Sources*, vol. 273, pp. 1136–1141, 2015.

[55] Z. W. Seh, H. Wang, N. Liu, G. Zheng, W. Li, H. Yao, and Y. Cui, "High-capacity Li_2S–graphene oxide composite cathodes with stable cycling performance," *Chemical Science*, vol. 5, no. 4, pp. 1396–1400, 2014.

[56] Y. Cui and Y. Fu, "Polysulfide transport through separators measured by a linear voltage sweep method," *Journal of Power Sources*, vol. 286, pp. 557–560, 2015.

[57] Y. V. Mikhaylik and J. R. Akridge, "Polysulfide shuttle study in the Li/S battery system," *Journal of the Electrochemical Society*, vol. 151, no. 11, pp. A1969–A1976, 2004.

[58] M. Armand and J.-M. Tarascon, "Building better batteries," *Nature*, vol. 451, no. 7179, pp. 652–657, 2008.

[59] F. Cheng, J. Liang, Z. Tao, and J. Chen, "Functional materials for rechargeable batteries," *Advanced Materials*, vol. 23, no. 15, pp. 1695–1715, 2011.

[60] V. Etacheri, R. Marom, R. Elazari, G. Salitra, and D. Aurbach, "Challenges in the development of advanced Li-ion batteries: a review," *Energy & Environmental Science*, vol. 4, no. 9, pp. 3243–3262, 2011.

[61] M. Armand, S. Grugeon, H. Vezin, S. Laruelle, P. Ribière, P. Poizot, and J.-M. Tarascon, "Conjugated dicarboxylate anodes for Li-ion batteries," *Nature Materials*, vol. 8, no. 2, pp. 120–125, 2009.

[62] Z. Song, Y. Qian, X. Liu, T. Zhang, Y. Zhu, H. Yu, M. Otani, and H. Zhou, "A quinone-based oligomeric lithium salt for superior Li–organic batteries," *Energy & Environmental Science*, vol. 7, no. 12, pp. 4077–4086, 2014.

[63] T. Nokami, T. Matsuo, Y. Inatomi, N. Hojo, T. Tsukagoshi, H. Yoshizawa, A. Shimizu, H. Kuramoto, K. Komae, H. Tsuyama *et al.*, "Polymer-bound pyrene-4, 5, 9, 10-tetraone for fast-charge and-discharge lithium-ion batteries with high capacity," *Journal of the American Chemical Society*, vol. 134, no. 48, pp. 19 694–19 700, 2012.

[64] W. Huang, Z. Zhu, L. Wang, S. Wang, H. Li, Z. Tao, J. Shi, L. Guan, and J. Chen, "Quasi-solid-state rechargeable lithium-ion batteries with a calix [4] quinone cathode and gel polymer electrolyte," *Angewandte Chemie*, vol. 125, no. 35, pp. 9332–9336, 2013.

[65] L. Zhao, J. Zhao, Y.-S. Hu, H. Li, Z. Zhou, M. Armand, and L. Chen, "Disodium terephthalate ($Na_2C_8H_4O_4$) as high performance anode material for low-cost room-temperature Sodium-Ion battery," *Advanced Energy Materials*, vol. 2, no. 8, pp. 962–965, 2012.

[66] S. Wang, L. Wang, Z. Zhu, Z. Hu, Q. Zhao, and J. Chen, "All organic Sodium-Ion batteries with $Na_4C_8H_2O_6$," *Angewandte Chemie International Edition*, vol. 53, no. 23, pp. 5892–5896, 2014.

[67] C. Luo, J. Wang, X. Fan, Y. Zhu, F. Han, L. Suo, and C. Wang, "Roll-to-roll fabrication of organic nanorod electrodes for sodium ion batteries," *Nano Energy*, vol. 13, pp. 537–545, 2015.

[68] H. Wu, S. A. Shevlin, Q. Meng, W. Guo, Y. Meng, K. Lu, Z. Wei, and Z. Guo, "Flexible and binder-free organic cathode for high-performance Lithium-Ion batteries," *Advanced Materials*, vol. 26, no. 20, pp. 3338–3343, 2014.

[69] S. J. Visco, C. C. Mailhe, L. C. De Jonghe, and M. B. Armand, "A novel class of organosulfur electrodes for energy storage," *Journal of The Electrochemical Society*, vol. 136, no. 3, pp. 661–664, 1989.

[70] M. Liu, S. J. Visco, and L. C. De Jonghe, "Electrode kinetics of organodisulfide cathodes for storage batteries," *Journal of The Electrochemical Society*, vol. 137, no. 3, pp. 750–759, 1990.

[71] S. J. Visco, M. Liu, and L. C. DeJonghe, "Ambient temperature high-rate lithium/organosulfur batteries," *Journal of the Electrochemical Society*, vol. 137, no. 4, pp. 1191–1192, 1990.

[72] M. Liu, S. J. Visco, and L. C. De Jonghe, "Novel solid redox polymerization electrodes all-solid-state, thin-film, rechargeable lithium batteries," *Journal of The Electrochemical Society*, vol. 138, no. 7, pp. 1891–1895, 1991.

[73] T. Sotomura, H. Uemachi, K. Takeyama, K. Naoi, and N. Oyama, "New organodisulfidepolyaniline composite cathode for secondary lithium battery," *Electrochimica Acta*, vol. 37, no. 10, pp. 1851–1854, 1992.

[74] N. Oyama, J. M. Pope, and T. Sotomura, "Effects of adding copper (ii) salt to organosulfur cathodes for rechargeable lithium batteries," *Journal of the Electrochemical Society*, vol. 144, no. 4, pp. L47–L51, 1997.

[75] K. Naoi, K.-i. Kawase, M. Mori, and M. Komiyama, "Electrochemistry of poly (2, 2-dithiodianiline): A new class of high energy conducting polymer interconnected with s–s bonds," *Journal of the Electrochemical Society*, vol. 144, no. 6, pp. L173–L175, 1997.

[76] L. Yu, X. Wang, J. Li, X. Jing, and F. Wang, "Enhanced redox processes of disulfides with partially N-methylated polyaniline," *Journal of Power Sources*, vol. 73, no. 2, pp. 261–265, 1998.

[77] N. Oyama, "Development of polymer-based lithium secondary battery," *Macromolecular Symposia*, vol. 159, no. 1, pp. 221–228, 2000.

[78] N. Oyama and O. Hatozaki, "Lithium polymer battery with high energy density," *Macromolecular Symposia*, vol. 156, no. 1, pp. 171–178, 2000.

[79] J. E. Park, S. Kim, S. Mihashi, O. Hatozaki, and N. Oyama, "Roles of metal nanoparticles on organosulfur-conducting polymer composites for lithium battery with high energy density," *Macromolecular Symposia*, vol. 186, no. 1, pp. 35–40, 2002.

[80] S.-R. Deng, L.-B. Kong, G.-Q. Hu, T. Wu, D. Li, Y.-H. Zhou, and Z.-Y. Li, "Benzene-based polyorganodisulfide cathode materials for secondary lithium batteries," *Electrochimica Acta*, vol. 51, no. 13, pp. 2589–2593, 2006.

[81] Y. Kiya, G. R. Hutchison, J. C. Henderson, T. Sarukawa, O. Hatozaki, N. Oyama, and H. D. Abruña, "Elucidation of the redox behavior of 2, 5-dimercapto-1, 3, 4-thiadiazole (DMcT) at poly (3, 4-ethylenedioxythiophene)(PEDOT)-modified electrodes and application of the DMcT-PEDOT composite cathodes to lithium/lithium ion batteries," *Langmuir*, vol. 22, no. 25, pp. 10 554–10 563, 2006.

[82] T. L. Pickering, K. Saunders, and A. V. Tobolsky, "Disproportionation of organic polysulfides," *Journal of the American Chemical Society*, vol. 89, no. 10, pp. 2364–2367, 1967.

[83] E. L. Clennan and K. L. Stensaas, "Recent progress in the synthesis, properties and reactions of trisulfanes and their oxides," *Organic Preparations and Procedures International*, vol. 30, no. 5, pp. 551–600, 1998.

[84] Y. Cui and Y. Fu, "Enhanced cyclability of Li/Polysulfide batteries by a polymer-modified carbon paper current collector," *ACS Applied Materials & Interfaces*, vol. 7, no. 36, pp. 20 369–20 376, 2015.

[85] S. S. Zhang, "Effect of discharge cutoff voltage on reversibility of lithium/sulfur batteries with $LiNO_3$-contained electrolyte," *Journal of The Electrochemical Society*, vol. 159, no. 7, pp. A920–A923, 2012.

[86] S. Zhang, "Role of $LiNO_3$ in rechargeable lithium/sulfur battery," *Electrochimica Acta*, vol. 70, pp. 344–348, 2012.

[87] M. Liu, S. J. Visco, and L. C. De Jonghe, "Electrochemical properties of organic disulfide/thiolate redox couples," *Journal of The Electrochemical Society*, vol. 136, no. 9, pp. 2570–2575, 1989.

[88] M. Wu, Y. Cui, and Y. Fu, "Li_2S nanocrystals confined in free-standing carbon paper for high performance Lithium–Sulfur batteries," *ACS Applied Materials & Interfaces*, vol. 7, no. 38, pp. 21 479–21 486, 2015.

[89] S. Chen, F. Dai, M. L. Gordin, Z. Yu, Y. Gao, J. Song, and D. Wang, "Functional organosulfide electrolyte promotes an alternate reaction pathway to achieve high performance in Lithium–Sulfur batteries," *Angewandte Chemie*, vol. 128, pp. 4303–4307, 2016.

[90] S. S. Zhang, "Improved cyclability of liquid electrolyte lithium/sulfur batteries by optimizing electrolyte/sulfur ratio," *Energies*, vol. 5, no. 12, pp. 5190–5197, 2012.

[91] M. Hagen, D. Hanselmann, K. Ahlbrecht, R. Maça, D. Gerber, and J. Tübke, "Lithium–Sulfur Cells: The gap between the state-of-the-art and the requirements for high energy battery cells," *Advanced Energy Materials*, vol. 5, no. 16, p. 1401986, 2015.

[92] C. Zu and A. Manthiram, "High-performance Li/dissolved polysulfide batteries with an advanced cathode structure and high sulfur content," *Advanced Energy Materials*, vol. 4, no. 18, p. 1400897, 2014.

[93] S.-H. Chung, C.-H. Chang, and A. Manthiram, "Robust, ultra-tough flexible cathodes for high-energy Li–S batteries," *Small*, vol. 12, pp. 939–950, 2015.

[94] S.-H. Chung, P. Han, R. Singhal, V. Kalra, and A. Manthiram, "Electrochemically stable rechargeable Lithium–Sulfur batteries with a microporous carbon nanofiber filter for polysulfide," *Advanced Energy Materials*, vol. 5, no. 18, p. 1500738, 2015.

[95] Q. Fan, W. Liu, Z. Weng, Y. Sun, and H. Wang, "Ternary hybrid material for high-performance Lithium–Sulfur battery," *Journal of the American Chemical Society*, vol. 137, no. 40, pp. 12 946–12 953, 2015.

[96] Q. Zhao, Y. Lu, Z. Zhu, Z. Tao, and J. Chen, "Rechargeable Lithium-Iodine batteries with iodine/nanoporous carbon cathode," *Nano Letters*, vol. 15, no. 9, pp. 5982–5987, 2015.